



JGR Space Physics

RESEARCH ARTICLE

10.1029/2024JA032535

Key Points:

- Satellite observations of neutral and electron densities provide an excellent means to examine the topside ionospheric response to wave driving in the lower atmosphere via large-scale wave structures
- Correlation analyses revealed that tides act as a mediator for the interaction and coupling between wavenumber structure patterns of density, which appear similar for narrow LT and magnetic LT differences
- CTMT results can generally explain the vertical coupling of the wavenumber structure of density caused by upward propagating tides originating from lower and middle atmospheric sources

Correspondence to:

S. M. Khadka, sovit.khadka@orionspace.com

Citation:

Khadka, S. M., Gasperini, F., Stolle, C., & Oberheide, J. (2024). Large-scale wavedriven interactions and plasma-neutral coupling in the low-latitude ionosphere-thermosphere. *Journal of Geophysical Research: Space Physics, 129*, e2024JA032535. https://doi.org/10.1029/2024JA032535

Received 9 FEB 2024 Accepted 7 MAY 2024

Author Contributions:

Conceptualization: Sovit M. Khadka, Federico Gasperini
Formal analysis: Sovit M. Khadka
Investigation: Sovit M. Khadka
Methodology: Sovit M. Khadka,
Federico Gasperini
Resources: Sovit M. Khadka,
Federico Gasperini
Software: Sovit M. Khadka
Writing – original draft: Sovit
M. Khadka
Writing – review & editing: Sovit
M. Khadka, Federico Gasperini,

Claudia Stolle, Jens Oberheide

© 2024. American Geophysical Union. All Rights Reserved.

Large-Scale Wave-Driven Interactions and Plasma-Neutral Coupling in the Low-Latitude Ionosphere-Thermosphere

Sovit M. Khadka¹, Federico Gasperini¹, Claudia Stolle², and Jens Oberheide³

¹Orion Space Solutions, Louisville, CO, USA, ²Leibniz Institute of Atmospheric Physics at the University of Rostock, Kühlungsborn, Germany, ³Department of Physics and Astronomy, Clemson University, Clemson, SC, USA

Abstract The plasma and neutral density variations, interactions and coupling processes within ±30° latitudes are examined concurrently by the DMSP-F18 and Swarm-C satellite during geomagnetically quiet years in 2020-2021. The wavenumber (WN) patterns are computed in the form of neutral and electron density for two altitudes and their latitudinal profiles are analyzed. We observe that the WN1 structure of the electron density has a significant seasonal dependence in the topside ionosphere and dominates all other structures but WN2 neutral density amplitude dominates all other structures in the middle thermosphere (~440 km). Additionally, we analyze vertical-temporal-latitudinal tidal structures from the Climatological Tidal Model of the Thermosphere (CTMT) to find evidence for the modulation of the large-scale waves (LSWs) neutral density structures. Through the examination of the in situ observational and modeling approaches, we show that the tidal contributors of WN structures obtained from CTMT can capture the influence of terrestrial sources on the WN structures of plasma-neutral density and imprint the corresponding vertical coupling in the IT system. Correlation analysis reveals that the amplitudes of the WN1 and WN3 structures of electron density in topside ionosphere and those of neutral density in the middle thermosphere show intermittent but significant correlations with each other, unlike the WN2 and WN4 structures. This study provides new insights into the topside ionospheric response to wave driving in the lower atmosphere, which ultimately improves our capability to understand the interaction and vertical coupling of large-scale structures, thereby advancing our predictive capabilities of space weather critical for satellite operations.

1. Introduction

Accurate understanding of the interaction between neutrals and plasma and their coupling via large-scale waves (LSWs) in the ionosphere-thermosphere (IT) region is crucial for predicting and mitigating space weather threats to satellite-based communication, and navigation, as well as radiation hazards to humans and avionics systems. A broad range of temporal and spatial events (e.g., gravity waves, sudden stratospheric warmings), generally modulated by solar and magnetospheric sources, makes the IT region a highly unstable system. Even without these intermittent-in-nature states, the IT system shows persistent variability that is largely influenced by terrestrial weather. The LSWs of lower atmospheric origin (neutrals, plasma, temperature, pressure, winds, etc.) most affecting the IT system have periodicities from 8 hr to a few days. A significant subset of this wave variability generated in the tropical troposphere propagates to higher altitudes, ultimately providing an opportunity for neutrals and plasma to interact and couple with each other.

Sun synchronous (non-Sun-synchronous) propagating tides are called migrating (nonmigrating) tides. This usually leads to the formation of the effects of migrating tides in day-night variations and the effects of nonmigrating tides in the longitudinal variations. We used the widely adopted tidal notation (e.g., Hagan & Forbes, 2002) for atmospheric tides in this study. As such, diurnal tides propagating eastward (westward) are denoted by DEs (DWs), where the ends with their absolute magnitude, s, is the zonal wavenumber. Tides with the zonal wavenumber positive integer "s" and negative integer "s" propagate westward and eastward, respectively. Similarly, for semidiurnal tides, the D is replaced by an S. If tidal oscillations are zonally symmetric, they are denoted by D0 (S0) for diurnal (semidiurnal) tides. The stationary planetary waves (SPW) with a zonal number s are referred to as SPWs. Solar atmospheric tides, related to global-scale variations of density, temperature, pressure, and wind waves with periods being solar day or their subharmonics, are responsible for interaction and coupling the lower and upper layers of the atmosphere. A variety of plasma-neutral coupling processes with a range of spatial and temporal scales cause the tropical troposphere variability to be mapped into the IT system (Gasperini et al., 2021; Oberheide et al., 2015). Due to the unique configuration of electric and magnetic field

KHADKA ET AL. 1 of 23

lines near the equator, much of the IT response to terrestrial weather occurs at low latitudes (<30°) and is driven by waves that are excited by deep convective processes in the tropical troposphere and that propagate upwards into the IT system (Gasperini et al., 2021; Khadka, 2018; Khadka et al., 2016; Oberheide & Forbes, 2008; Williams & Avery, 1996). Tides can be excited by orographic features (Forbes & Garrett, 1979), and by deep convective forcing where tidal heating occurs because of cloud droplet formation (i.e., latent heat release during the vapor to liquid phase transition). Another possible sources of nonmigrating tides are nonlinear interactions between stationary planetary wave (SPW) and migrating tides or tidal/tidal interactions (Lieberman et al., 2004 and references therein). Non-linear interactions in the neutral atmosphere with planetary waves generate child waves capable of modulating amplitude of original or parent tidal waves (Chang et al., 2013; Yue et al., 2013). The upward propagating waves present in the tropical troposphere, mesosphere/lower thermosphere (MLT) can impact upper atmospheric temperature, wind, and composition structures (Gasperini et al., 2023; Krier et al., 2021). Vertically propagating tides have profound influences on the transport of energy and momentum from their sources into the MLT region (80-120 km altitude ranges) and beyond until they dissipate and deposit energy and momentum into the background IT (Jones et al., 2014; Liu et al., 2021). As tidal waves propagate vertically upward, their amplitudes increase with decreasing background atmospheric density to keep the conservation of wave energy. The tidal energy is frequently redistributed among different tidal components in some wave-wave interactions, but some components do not have enough spatial overlap to transfer energy. For example, DE3, the most prominent nonmigrating tidal components, have mode interactions that transfer energy within one tidal component, depending on background conditions (Zhang et al., 2012). A few waves from the tropical wave system, which propagates and affects the IT system, tend to modify satellite drag (Forbes et al., 2009; Gasperini et al., 2015, 2017; Oberheide et al., 2009) ionospheric densities (Chang et al., 2011; Gasperini et al., 2021; Gu et al., 2014; Pedatella & Forbes, 2009), column number density (O/N₂) ratio (Kil et al., 2013; Qian et al., 2022) F-region dynamo electric fields (Lin et al., 2007), and even GPS signal fluctuations (S4 index) to a significant degree (Liu et al., 2013).

A significant portion of solar tides present in the thermosphere are originated in the lower and middle atmosphere (Forbes, 2000; Fritts & Alexander, 2003; Hagan & Forbes, 2002; Hagan & Roble, 2001; Huang et al., 2012) then propagate vertically from below or spread latitudinally via ducting within the middle and upper atmosphere (Jarvis, 2006; Jones et al., 2019; McLandress, 2002; Sato et al., 2009; Wang et al., 2021; Zeng et al., 2008). Some of these waves are also generated in situ by gravity waves or tides modulated by planetary waves encountered at lower altitudes causing wave-wave interactions (Jarvis, 2006; Lawrence & Jarvis, 2001, 2003; Smith, 2003). This global scale interaction and vertical propagation of waves affects the local neutrals in the lower thermosphere and the local plasma in the ionosphere (Smith, 2012; Triplett et al., 2019; Vincent, 2015; Yue et al., 2016). Numerous modeling studies (Chang et al., 2008; Fang et al., 2013; Hagan & Forbes, 2002; Oberheide et al., 2011a; Yamazaki & Richmond, 2013), observational studies from ground-based instruments (Forbes, 2000; Gong & Zhou, 2011; Huang et al., 2012; Negrea et al., 2016), and satellite-based (Forbes et al., 2017; Gasperini et al., 2015, 2022; McLandress et al., 1996; Mukhtarov & Pancheva, 2011) data analyses have focused on atmospheric tides and their influence in the dynamics, structure, and variability of the IT system. Ground-based observations provide an important perspective on the local behavior or short-term changes in tidal waves, whereas satellite observations are the best way to examine global or large-scale structures and hence distinguish their different tidal components in the IT system. Although the efforts of these studies made some progress on addressing these topics, especially recent IT-dedicated satellite missions, detailed understanding on the role played by upward propagating tides and their connection to the longitudinal structure of waves in the IT system is still a dashing question to the science community. Due to the sparsity of concurrent global observations, the full characterization of the sources of dayto-day variability of tidal waves of tropical tropospheric origin, including nonlinear interactions, coupling between different atmospheric regions, and their impacts on the low-latitude IT system, is very limited (Gasperini et al., 2022). If the E-region dynamo electric fields are not dominated by changes in geomagnetic activity, the upward propagating tides are responsible for the longitudinal variability but the effectiveness of these tides to produce longitudinal structures in the ionosphere has yet fully to be determined (Gasperini et al., 2018; Pedatella et al., 2008). The modeling effort on this case reveals that solar thermal tides generated in the troposphere can noticeably induce longitudinal variability in the ionosphere F-region (Hagan et al., 2007) and if these tides are capable of inducing a longitudinal structure in the dynamo electric fields, a similar type of structure should exist in ionospheric electron density structures (England et al., 2008). The modulation of the neutral density in the middle thermosphere by tides ultimately controls the formation of the ionospheric height. The collective effects of all tidal components in producing significant longitudinal tidal variability depends on the constructive and

KHADKA ET AL. 2 of 23

destructive interference and different vertical displacement effects that occur from one longitude sector to the next (Cahoy et al., 2006; Forbes et al., 2008).

Admittedly, the sources and physical mechanisms of interaction and coupling between plasma and neutral, including forcing from above, below, and internal modifications, have been studied extensively from observational and model perspectives for several decades, but the details on topside ionospheric response to wave driving in the lower atmosphere is overlooked and coupling mechanism of LSWs via tidal waves in the "IT gap" regions, particularly above 400 km, are still not clear. In addition, the mechanisms by which the tidal signatures are manifest in the tropical troposphere are generally well defined, but their IT response is still being debated. In the same vein, the availability of concurrent Defense Meteorological Satellite Program (DMSP) and Swarm-C, a European Space Agency (ESA) Earth Explorer mission, satellite observations at two different altitudes, 840 and 440 km respectively, and an empirical model utilizing Hough Mode Extensions (HMEs), and Climatological Tidal Model of the Thermosphere (CTMT) simulations during the solar minimum and geomagnetically quiescent years (2020 and 2021) for similar F10.7 conditions, provides an excellent opportunity to explore the topside ionospheric response to wave driving in the lower atmosphere. The primary goal is to understand how globalscale waves and their interactions couple tropical tropospheric variability with neutral and plasma density variability in the IT system. Most observational studies, including those cited above, present very limited evidence of interaction and coupling between plasma and neutral in global scales via terrestrial sources in the middle/ upper thermosphere and topside ionosphere. Relative to prior studies, our analysis extends the characterization of tides and their role in the interaction and coupling of the large-scale wave structures of density from lower/middle thermosphere to the topside ionosphere using DMSP data above 800 km altitude, that is, much higher than most previous IT coupling studies focusing on global-scale impacts at lower latitudes. Additionally, however, very limited work has been done on investigating the WNS of density and their dynamics using satellites data, particularly of DMSP and Swarm satellites, herein we extract wave number structures of neutral and plasma density from observations using a Swarm-C and DMSP-F18 satellites respectively and examine their interactions and coupling using contribution of the tidal components obtained from the CTMT model simulations. Notwithstanding under nearly constant solar and geomagnetic activity levels, our analysis focusing on quiet periods emphasizes the significance of lower atmospheric processes, particularly terrestrial sources. A correlation analysis has been performed between the electrodynamics of the WNS of plasma in the topside ionosphere and those of the neutral particles from the middle thermosphere, and then the level of correlation is quantified. We identify the possible cause-effect factors for the vertical propagation of LSWs in the IT system from below at tropical latitudes that trigger the variability, interaction, and coupling between plasma and neutrals.

The organization of this manuscript is as follows: in Section 1 we give an overview of related previous studies, current research efforts to address scientific questions, some unanswered questions, and our efforts to address these questions. Section 2 we describe the data sources, briefly overview these observational data sets, the model used, analysis techniques, and the method of analysis. Section 3 provides details on the analysis and the results revealed from the data and the model. Section 4 focuses on the discussion and interpretation of the output from Section 3, and Section 5 summarizes the research investigation and the main conclusions.

2. Data Sources, Model, and Approach of Analysis

The neutral and electron density measurements from Swarm-C and DMSP-F18 satellites, respectively, for 2 years (2020 and 2021) solar quiet days are used to study the large-scale wave patterns and their role in the interaction and coupling via thermal tides in the low-latitude region. Solar thermal tides are global-scale oscillations, and therefore a satellite perspective of the tidal fields presents multifarious advantages (Zhang et al., 2006). We discuss the in situ DMSP-F18 and Swarm-C data processing techniques to calculate wavenumber structures and to take advantage of the concurrent (same Universal Time but different geographical locations) measurements of electron and neutral density at two different altitudes along their ascending paths in the IT regions. Additionally, the diurnal and semidiurnal tidal components obtained from the CTMT are used to interpret the interaction and coupling mechanism between plasma and neutral under the aforementioned conditions.

2.1. Background Geomagnetic Conditions

Geomagnetic activity can be represented as the occurrence of K-variations (e.g., geomagnetic pulsations, bays or substorms, sudden commencements, geomagnetic storms, etc.). The purpose of the Kp index, and derived products

KHADKA ET AL. 3 of 23

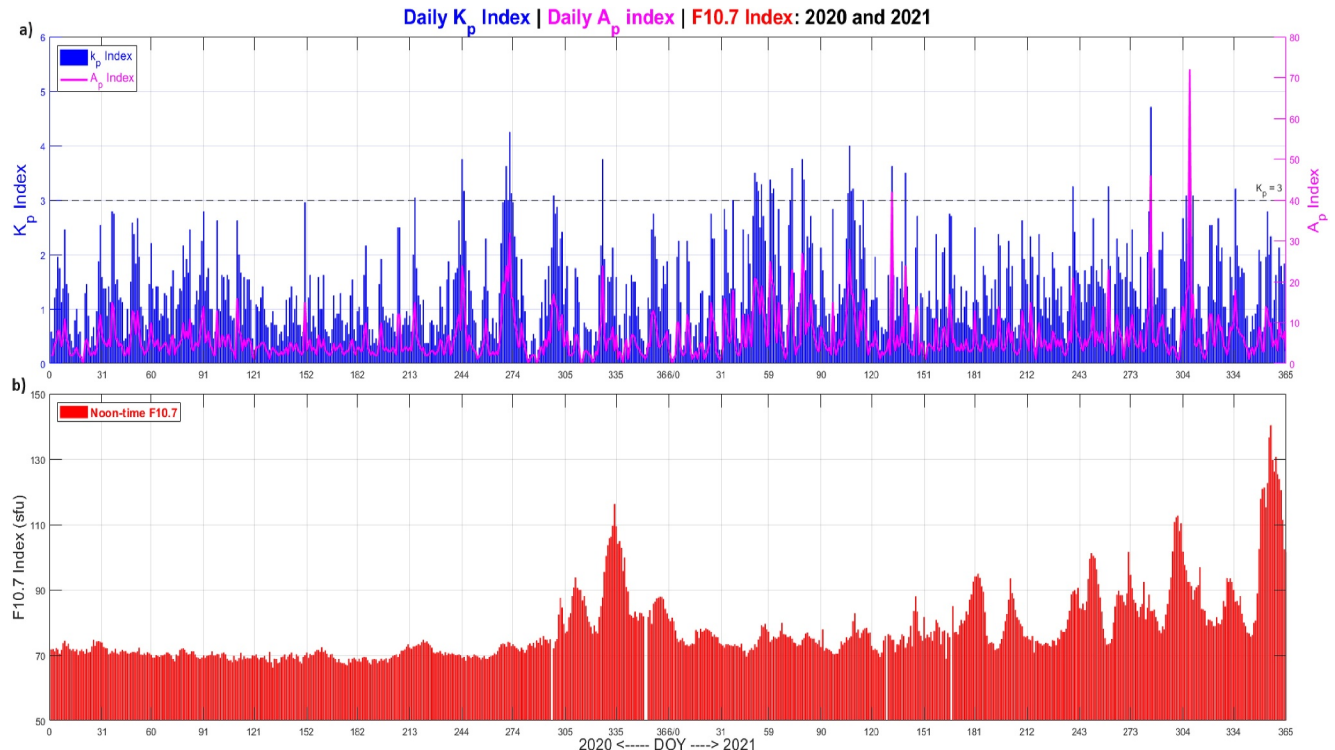


Figure 1. Geomagnetic Conditions: (a) Day of the year (DOY) distributions of the daily average Kp index (blue bars) and Ap index (magenta curves) for 2020 and 2021. The dotted horizontal line represents the threshold line corresponding to Kp = 3, and (b) the noontime solar radio flux F10.7 shown in the bottom panel. Only satellites data falling below the threshold line ($Kp \le 3$) are used for analysis in this project.

are to monitor sub-auroral geomagnetic disturbances on a global scale which are particularly important for space weather research and services (Matzka et al., 2021). This analysis focuses on the geomagnetically quiet days during solar minimum years, 2020 and 2021. To specify the geomagnetic condition, Kp and Ap indices are chosen. Due to the impact of the recovery phase of geomagnetic storm, the tidal perturbation due to storms cannot completely be excluded by choosing low Kp values but their impacts can be minimized. We selected geomagnetically quiet days (daily average Kp \leq 3) for analysis, aiming for minimal perturbations due to the storm related influences on the large-scale structures of density. Figures 1a and 1b show variations of these indices for 2 years and the flux density of solar radio emissions at a wavelength of 10.7 cm that characterizes solar activity levels, respectively.

2.2. Observational Data Sources

2.2.1. Defense Meteorological Satellite Program (DMSP)

The sparse study of the topside ionosphere (above 800 km) is generally due to limited data availability in comparison with the lower part of the ionosphere (below 400 km). This deficiency is somewhat addressed by a constellation, or a series of satellite launches in the Defense Meteorological Satellite Program (DMSP). During its operation for over 50 years, numerous studies on the topside ionosphere have been carried out using the DMSP data but there has been very limited analysis done from a tidal perspective. This program provides strategic and tactical weather prediction to aid the US military in planning operations at sea, on land and in the air. However, a significant number of satellites (F1–F15 and F19) in the series of the DMSP program have already been retired, leaving the currently operational in the series with the data accessible from only three spacecrafts (F16–F18), with different orbital altitudes and local times (Cai et al., 2019; Kramer, 2002). DMSP-F18 has two local times (LTs) of ascending (~17 Magnetic LT) and descending (~05 Magnetic LT) nodes at the equator crossing that remain relatively constant throughout the lifetime of the satellite and merely varies a few minutes during each year due to a slight non-uniformity in the Earth's orbit around the Sun. The Air Force has flown the Special Sensor for Ions, Electrons and Scintillation (SSIES) instrument package (Hairston & Heelis, 1996; Hairston et al., 1998) onboard the DMSP spacecrafts in sun-synchronous near-polar orbits with an orbital period of about 101 min and

KHADKA ET AL. 4 of 23

inclination near of 99° at altitudes near 840 km since the late 1980s. This instrument provides numerous measurements, among others, of ion density. The DMSP electron/ion density data is publicly available via the CE-DAR Madrigal database and provides us an opportunity to study the possible interaction and coupling between the topside ionosphere and middle thermosphere during the quiet days studies. In this study, we use topside ionospheric electron number density (N_e) from the DMSP-F18 data, extract wavenumber structures, and analyze its variations along ascending segments with respect to geomagnetic coordinates under undisturbed conditions during solar minimum years.

2.2.2. Swarm-C Satellite

The ESA's Swarm constellation mission for Earth Observation consists of three identical satellites, Swarm-A (Alpha), Swarm-B (Bravo), and Swarm-C (Charlie). This constellation was launched in November 2013 into near-polar circular orbits. Swarm-A and Swarm-C orbit side by side at an altitude of ~450 km with an inclination angle of 87.5°, and Swarm-B orbits at an altitude of ~510 km with an inclination angle of 88° providing fully global coverage with a mean altitude that decreased to ~440 km by 2020. This constellation is equipped with multiple instruments and provides precise simultaneous measurements of the magnetic field and various ionospheric parameters over different regions of the Earth through a number of payloads onboard each satellite (Friis-Christensen et al., 2008). Besides the primary research objectives of the Swarm mission, which are investigations of the electrodynamics of the Earth's core to its magnetosphere and ionosphere, mission data can also be used for space weather, climatology, modeling, and vertical coupling related studies in the upper atmosphere (Schrijver et al., 2015; Wood et al., 2022).

Swarm-C carries onboard an accelerometer and GPS receiver package as part of its scientific payload that are used to estimate total mass density (Siemes et al., 2016). For studying the dynamics of the upper atmosphere, which results from a complex interaction between the charged particles and the neutrals in the ambient magnetic field, the Precise orbit determination (POD) and Thermospheric Density and Wind (TDW) chains suite on board of the Swarm satellites allow the derivation of the thermospheric neutral density of the upper atmosphere (van den IJssel et al., 2020; Visser et al., 2013). The POD is necessary for geolocating the observations taken by the scientific instruments on board of the Swarm satellites. The POD-derived neutral density product is publicly available. For Swarm-C satellite, during 2020–2021, the local time at the ascending and descending trajectories slowly drifts and takes around 133–135 days to cover all 24 hr of local times. Swarm-C has a duration of about 90 min for one orbit and completes nearly 15 orbital cycles every 24 hr. Referring to these orbital parameters, the satellite drifts about 2 hr local time every 11 days. We utilize the POD neutral density (in situ, ~440 km) data from Swarm-C to derive large-scale wave structure amplitudes for the ascending path (only along red traces in Figure 2) during solar minimum years 2020 and 2021.

2.3. Climatological Model and Limitations

We employed the Climatological Tidal Model of the Thermosphere (CTMT) (Oberheide et al., 2011a) to elucidate the thermospheric variability resulting from upward propagating tides originated from below the mesosphere lower-thermosphere (MLT) region/lower atmosphere. This model is based on observations of tidal temperatures and winds in the MLT region from the Sounding of the Atmosphere using Broadband Emission Radiometer (SABER) and TIMED Doppler Interferometer (TIDI) instruments onboard the Thermosphere Ionosphere Mesosphere Energetics Dynamics (TIMED) satellite, is extrapolated into the thermosphere using HME modeling approach (Forbes & Hagan, 1982; Forbes et al., 2014; Svoboda et al., 2005), and provides the global behavior of vertically propagating tides in the thermosphere of the altitude and latitude ranges of 0–400 km and pole to pole respectively. In this climatological model, the monthly 6 (8) most important diurnal (semidiurnal) migrating and nonmigrating tidal components are obtained by compiling an average of about 6 years (2002–2008) of the TIMED observations.

As outlined in Oberheide et al. (2011a), the CTMT is well-suited for contributions from solar radiation absorption in the troposphere and stratosphere, tropospheric latent heat release, and non-linear wave-wave interactions occurring in the MLT or below and is valid well for a low solar radio flux (F10.7 = $110 \, \text{sfu}$) conditions. Despite these performances, CTMT cannot capture the in situ thermospheric tidal forcing via migrating tides due to the absorption of solar EUV radiation, and nonmigrating tides by nonlinear interaction processes. For example, the modulation of the migrating diurnal tides that produces nonmigrating tides as secondary waves in the latter case

KHADKA ET AL. 5 of 23

21699402, 2024, 5, Downloaded from https://agupubs.onlinelibrary.wiley.com/doi/10.1029/2024/A032535 by Clemson University, Wiley Online Library on [28/04/2025]. See the Terms and Conditions (https://onlinelibrary.wiley.com/doi/10.1029/2024/A032535 by Clemson University, Wiley Online Library on [28/04/2025]. See the Terms and Conditions (https://onlinelibrary.wiley.com/doi/10.1029/2024/A032535 by Clemson University, Wiley Online Library on [28/04/2025]. See the Terms and Conditions (https://onlinelibrary.wiley.com/doi/10.1029/2024/A032535 by Clemson University, Wiley Online Library on [28/04/2025]. See the Terms and Conditions (https://onlinelibrary.wiley.com/doi/10.1029/2024/A032535 by Clemson University, Wiley Online Library on [28/04/2025]. See the Terms and Conditions (https://onlinelibrary.wiley.com/doi/10.1029/2024/A032535 by Clemson University, Wiley Online Library on [28/04/2025]. See the Terms and Conditions (https://onlinelibrary.wiley.com/doi/10.1029/2024/A032535 by Clemson University).

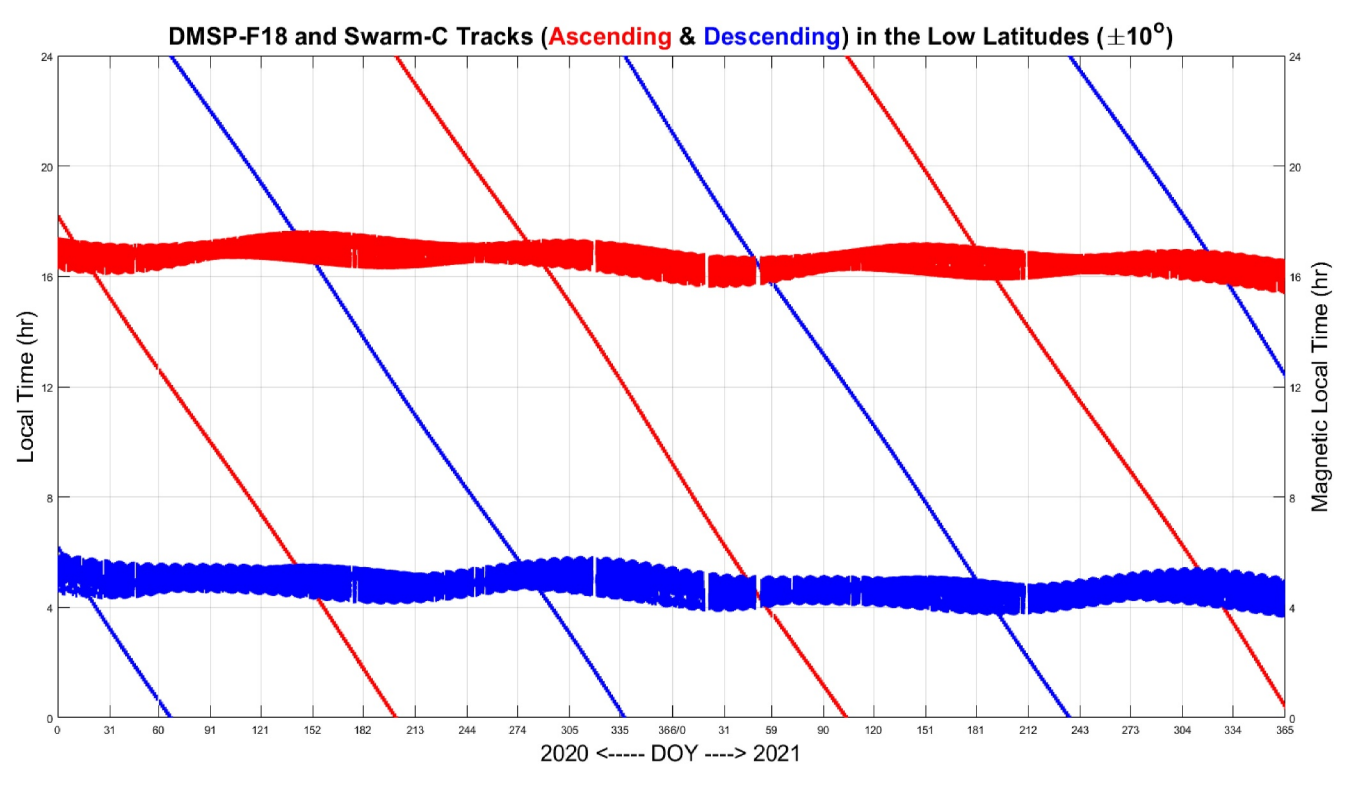


Figure 2. Satellites paths about solar and magnetic local times at the equator: Geometry of the satellite tracks for Swarm-C (tilted lines) and DMSP-F18 (horizontal curves) satellites over the low-latitude (±10°) region. The left vertical axis corresponds to Swarm-C whereas that in the right is for DMSP-F18 satellite data. The red (blue) lines represent the ascending (descending) paths of the satellites during their equatorial crossing. The ascending and descending paths are here chosen with reference to the argument of latitude and magnetic LT (mLT) for Swarm-C and DMSP-F18 satellites respectively. Only satellite data corresponding to ascending tracks of satellites are used for analysis to study day-to-day variability (see Section 2.4 for details) in this project. The narrow gaps in the curves represent either the unavailability of data points or are intentionally suppressed to remove the off-pattern data.

due to the offset between the geographical and geomagnetic equator cannot be incorporated in this model. The longitudinal ionospheric variability can produce significant D0 and DW2 tidal components through ion drag interactions involving the DW1 excited in situ in the thermosphere during solar activity conditions (Jones et al., 2013). CTMT has been successful in interpretating the Michelson Interferometer for Global Highresolution Thermospheric Imaging (MIGHTI) instrument on the Ionospheric CONnections (ICON)-derived zonal and meridional wind diurnal/semidiurnal tidal amplitudes for viscous dissipation and vertical coupling during solar low conditions (Forbes et al., 2022; Gasperini et al., 2023), but without in situ sources of excitation due to tide-tide or tide-ion drag nonlinear interactions. Even though the lower thermospheric tidal amplitudes are often larger in ICON/MIGHTI than CTMT, their structures and seasonal variations are in good agreement (Yamazaki et al., 2023). CTMT tidal components have been used and compared to many observational studies, in particular satellite observations (e.g., Forbes et al., 2012, 2014, 2022; Gasperini et al., 2023; Lieberman et al., 2013; Molina & Scherliess, 2023). Along the same vein, we use contribution of 14 diurnal and semidiurnal components obtained from CTMT to examine the role and contribution of terrestrial sources and forcing from bottom for the scenario of amplitudes of wave number structures of densities derived from Swarm-C and DMSP-F18 data in the low-latitude IT regions for days with geomagnetic activity index Kp below or equal to 3 ($K_p \le 3$).

2.4. Extraction of Wave Number Structures From Satellite Data

This subsection discusses how the large-scale wave structure of plasma and neutral density of satellite data collected by the DMSP-F18 and Swarm-C satellites are extracted. Satellite observations are the best way to study large-scale structures of density, temperature, wind in the upper atmosphere; and the data from these observations can be used to examine the vertical, meridional, and zonal structures of tidal wave patterns (Forbes & Wu, 2006; Forbes et al., 2008; Gasperini et al., 2021, 2023; McLandress et al., 1996; Pirscher et al., 2010; Wu et al., 2008;

KHADKA ET AL. 6 of 23

Yamazaki et al., 2023; Yuan et al., 2021; Zhang et al., 2006). The results presented here quantify the amplitudes of density wave structures in the upper atmosphere, based on the following approach that we adopted.

In this investigation, we chose the solar minimum years of 2020 and 2021, select geomagnetically quiet days $(K_p \le 3)$, and restrict only the ascending segments of satellite data for the analysis. For that purpose, the Swarm neutral density and DMSP electron density data are categorized and processed for five different latitudinal intervals, 20°N-30°N, 10°N-20°N, 10°N to 10°S, 10°S-20°S, and 20°S-30°S, which are referred to as 25°N, 15°N, 0° equator, 15°S, and 25°S, respectively, in this manuscript. We have analyzed the data and found that there is no significant difference in IT parameters between the 20° band at the equator and other bands, which are 10° wide. The geographic and geomagnetic latitudinal intervals are chosen for Swarm-C neutral and DMSP-F18 electron density data, respectively. This analysis focuses on solar and geomagnetic quiescent conditions to examine the role of terrestrial sources to the IT coupling. For each of those latitudinal intervals, the data corresponding to the days with daily average Kp > 3 are removed to restrict the analysis to quiet conditions. Only satellites data falling under the threshold line ($Kp \le 3$), represented by the dotted horizontal line in Figure 1a, are used for analysis. To simplify the data processing, the next criterion for data selection is the range of the points where a satellite orbit crosses a reference plane. For Swarm-C, the argument of latitude is taken as a reference to choose the ascending and descending paths. The angle along the satellite orbit, measured from the ascending node, so that 0° and 180° correspond to the ascending and descending equator crossings, respectively, while 90° and 270° correspond to the northern- and southernmost points in the orbit is called argument of latitude (Siemes et al., 2016). Similarly, for DMSP-F18 satellites, magnetic local time (mLT) is considered as a reference to choose the ascending (17 mLT) and descending (05 mLT) trajectories.

In general, tides are generated by the periodic heating of the Earth's daytime side atmosphere. Our analysis focuses on daytime, and hence along the ascending path of the satellite when the mean neutral density is largest, and the E-region dynamo is most effective (Forbes et al., 2018; Immel et al., 2018). To elucidate clear pictures of interaction and coupling phenomena, we only use satellite data corresponding to ascending path (along the red segments in Figure 2) path of both Swarm-C and DMSP-F18 satellites. We use WN structures on fixed LT space instead of tidal spectra to get day-to-day resolution. By considering only the ascending node, the LT variation within the 15-day interval is negligible, and hence we approximate it to be constant. Under the fixed LT approximation, migrating tides are largely absent in the WN fits, and the LT is not considered to be a significant factor for non-migrating tides, which are the focus of this study. Furthermore, the satellite's descending nodes (from the North Pole toward the South Pole) generally produce consistent results with those observed during the ascending nodes (from the South Pole toward the North Pole) with a 12-hr phase difference. Further, data binning is done on a daily (for available days) basis. In each daily bin, there are at least 18-24 data points. To put it another way, we select one data point within each 60-90-min window to ensure that there are enough data points to evaluate wavenumber patterns. After this, we get a desired set of DOY profile of density for $\pm 180^{\circ}$ longitudes for the WN structure analysis. This provides complete longitude coverage, which is one of the requirements to extract tidal characteristics of large-scale wave structures. As we discussed above, global oscillations of solar tides of density fields induced by the daily cyclic absorption of solar energy show the period equal to subharmonics of solar day in the upper atmosphere. Those harmonics fits of density waves are done in longitude using Equation 1 along ascending orbit node data. Then, the amplitudes of waves of zonal wavenumber 1-4 patterns (WN1-WN4) of neutral and electron density are evaluated using Swam-C and DMSP-F18 data, respectively.

$$y(\lambda)_{fit} = A_0 + \sum_{k=1}^{4} A_k \cos\left(\frac{2\pi}{360} \mathbf{k} (\lambda - \varphi_k)\right)$$
 (1)

In Equation 1, the variable A_0 denotes the mean amplitude of density waves, λ denotes the longitude in degrees. A_k and ϕ_k represent the amplitude and phase of the density wavenumber \mathbf{k} pattern, respectively. Different tidal components are included within each of the WN structures. A WN1 with fixed local time can be attributed either D0 or SW1. For instance, as presented in Table 1, WN4 represents the cumulative effect of DW5, DE3, SW6, SE2, SPW4, etc., which will be discussed in detail in the following sections.

Importantly, during the fitting, we use the 15-day sliding window technique and compute amplitude of WN1–WN4 structures from electron and neutral density data. Applying this methodology to electron and neutral density measurements from the DMSP-F18 and Swarm-C, we evaluate the daily profile of amplitude of the WN structures for 2020 and 2021 using fit formula Equation 1. The sliding window technique allows systems to break

KHADKA ET AL. 7 of 23

2169902, 2024, 5, Downloaded from https://agupubs.onlinelibrary.wiley.com/doi/10.1029/2024/032535 by Clemson University, Wiley Online Library on [2804/2025], See the Terms and Conditions (https://onlinelibrary.wiley.com/ems-and-conditions) on Wiley Online Library for rules of use; OA articles are governed by the applicable Creative Commons Licensia

Table 1
Contributing Tidal and Stationary Wave Components for Wavenumber Structures

WN Patterns	Contributing Wave Components for WN Structures				
WN1	DW2	D0	SW3	SW1	SPW1
WN2	DW3	DE1	SW4	S0	SPW2
WN3	DW4	DE2	SW5	SE1	SPW3
WN4	DW5	DE3	SW6	SE2	SPW4

Note. The shaded wave components in Table 1 are the potential sources of the WN1-WN4 structures available with CTMT.

down information into smaller blocks for more detailed analysis (Jaén-Vargas et al., 2022). However, the basic approach to sliding window data processing is to recompute the specific window slides, the data point within the window size might not be equally sampled in our case. This is because we constrained the data set in various desired regimes, for example, latitudes, quiet days, and ascending portion of satellites for the analysis. Thus, the aim for choosing the 15-day sliding window technique is to ensure that there are enough data points to accomplish the fit, reduce noise, and fill data gaps for nearly fixed local time. While presenting the results, we further restrict

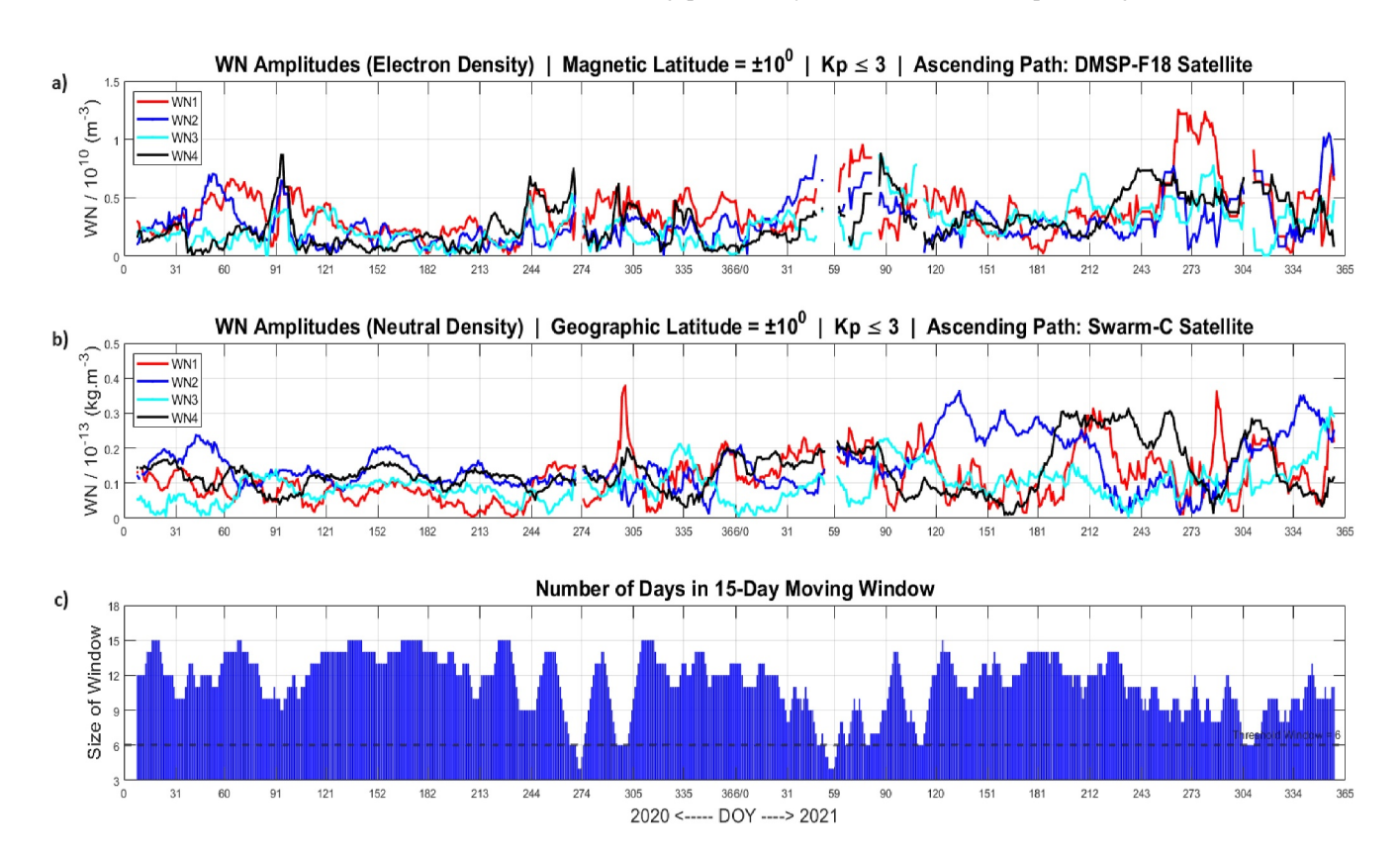


Figure 3. Wavenumber structures and the size of sliding window: Absolute wave number amplitudes of (a) electron density (in units of 10^{10} /m³) from DMSP-F18 and (b) neutral density (in units of 10^{-13} kg/m³) from Swarm-C satellites during equatorial ($\pm 10^{\circ}$) crossing along their ascending segment during geomagnetically quiet ($\text{Kp} \leq 3$) days of solar minimum years 2020 and 2021. The red, blue, cyan, and black curves in these panels represent the DOY versus amplitudes of the WN1, WN2, WN3, and WN4 of the density structures, respectively, evaluated from in situ data measurements. The panel (c) shows the size of sliding window (15-day) throughout the investigation whereas the dotted black line represents the threshold (40%) of the size of moving window.

KHADKA ET AL. 8 of 23

the wave number profiles by choosing a threshold size for the sliding window (15-day). If availability of data is only for 6 days (40%) or less in a 15-day sliding window, the wave number structures are ignored for that case. The top two panels in Figure 3 show the absolute WN1–WN4 amplitudes patterns of (a) DMSP-F18 electron, and (b) Swarm-C neutral density in the geomagnetic and geographic equatorial latitude region ($\pm 10^{\circ}$), respectively, for the 2 years using aforementioned methods. The small breaks in the WN curves refer to data points below threshold of the size of window separated by the dotted black line in the bottom panel of Figure 3.

Further, the results presented in top panel of Figure 3 show that the WN structures in the topside ionosphere are dominated by WN1 most of the time and intermittently by WN4 whereas that in lower/middle thermosphere, in second panel, are WN2 and WN4. Additionally, the periodicity of the large-scale structures of both neutral and electron density are closely related to short-term periodic variation in solar radiation which corresponds to approximately 27-day synodic rotation period of the Sun. At a first look, the first panel in Figure 3 shows that the absolute WN1 amplitude of electron density is the biggest compared to all other amplitudes throughout the years. But the second panel in Figure 3 demonstrates strong wave number amplitudes WN2 and WN4 of neutral density during most of the time during both years, 2020 and 2021. It also seems that WN2 neutral density amplitude in 3 (b) dominates all other structures near February and June in 2020 and May, June, and December of 2021. WN1 and WN4 become prominent towards the end of both 2020 and 2021, while WN2 regained its leading role at the end of 2021. According to Garner et al. (2010), the DMSP-F18 plasma density above 200 cm⁻³ is valid. In contrast, Visser et al. (2013), report that comparisons with physical and empirical models indicate errors less than ~11% for Swarm satellite data. The driving factors behind this behavior of WN amplitudes structure of electron and neutral density in the equatorial latitudes will be discussed in the following sections.

In fact, WN structures are superpositions of various tidal and stationary planetary waves. Referring to Häusler and Lühr (2009), potential wave sources of the WN1-WN4 structures are summarized in Table 1. The shaded wave components in Table 1 are the potential sources of the WN1-WN4 structures available with CTMT outputs. The details on the superposition of the available wave components with CTMT and reconstructed WN1-WN4 structures are discussed in Section 3.3.

3. Analysis and Results

The structure, interaction, and coupling of large-scale waves (LSWs) in plasma and neutral densities are investigated using satellite observations at two different altitudes, topside ionosphere (~840 km), and middle thermosphere (~440 km) under identical conditions (similar latitudes and quiet days). Observation-based climatological tidal model studies have revealed that migrating and nonmigrating diurnal and semidiurnal tides from 80 to 400 km altitudes and pole-to-pole for moderate solar flux conditions have significant influences on interaction and vertical coupling of the large-scale structures. Even though many studies reveal evidence of the interaction and coupling of the LSWs, their sources, drivers, and propagation are still in debate. Our analyses address such few questions with satellite measurement and from a modeling perspective. The focus is on analyzing the contribution of terrestrial sources on the measured density wave structures in the low-latitude IT system.

3.1. DMSP-F18 Electron Density

Referring to the method described in Section 2.4, the absolute amplitude of wave number structures during solar minimum years (2020 and 2021) derived from DMSP-F18 in situ measurement of electron density data at altitudes of 840 km for quiet days in the low-latitude (within 30°N–30°S) sector along ascending segment of satellite path are presented as a surface contour plot in Figure 4. From top to bottom, the four panels in Figure 4, display the WN1–WN4 variations, respectively, as a function of geomagnetic latitudes and day of the year (DOY) of 2020 and 2021. Similar to the electron density WN amplitudes presented in Figure 3a for equatorial latitude interval, $10^{\circ}N-10^{\circ}S$ (for 0°), we evaluate all (WN1–WN4) amplitudes using Equation 1 for other latitudinal intervals, $20^{\circ}N-30^{\circ}N$, $10^{\circ}N-20^{\circ}N$, $10^{\circ}S-20^{\circ}S$, and $20^{\circ}S-30^{\circ}S$ that correspond to the amplitudes for $+25^{\circ}$, $+15^{\circ}$, -15° , and -25° , respectively. These amplitudes of electron density WN amplitudes are collectively presented as contour subplots in Figure 4.

It can be inferred from the top panel of Figure 4 that the WN1 displays higher values than other WN patterns during summer season in both northern and southern hemispheres. An antisymmetric structure can clearly be seen in the magnitude of WN1 strengths and seems to follow seasonal patterns. A stronger WN1 is seen extended into

KHADKA ET AL. 9 of 23



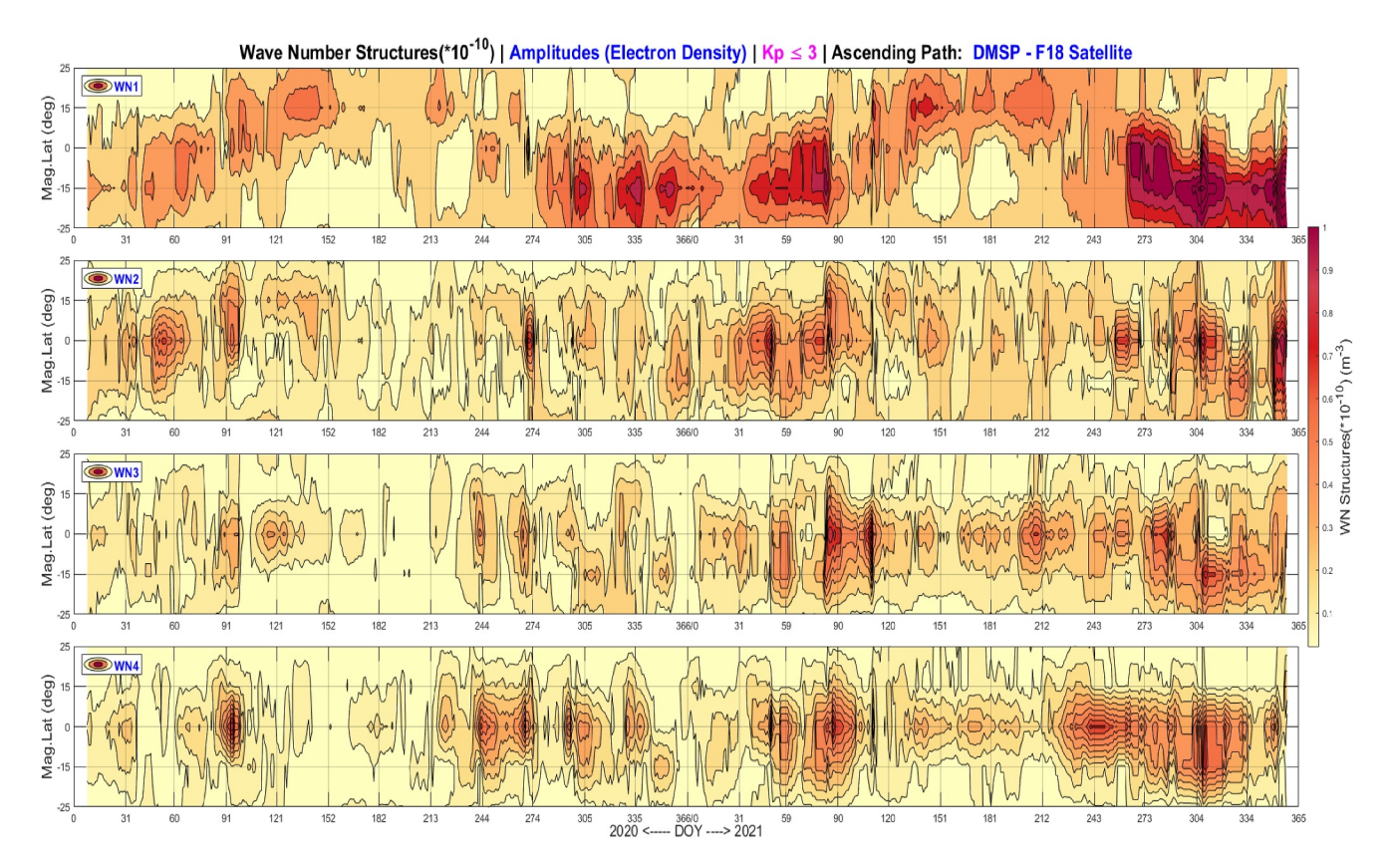


Figure 4. WNS from DMSP-F18: The DOY versus magnetic latitude distribution of the absolute amplitude of the wave number structures of electron density obtained from DMSP-F18 observations at 840 km altitude. Each panel (1st–4th) from top to bottom represents the contour (DOY vs. magnetic latitude) subplot of WN1-WN4 structures, respectively, in the low-latitude $(\pm 30^{\circ})$ region. These contour subplots are obtained by applying 15-day moving windows and including only geomagnetically quiet (Kp \leq 3) days data corresponding to ascending paths (along red lines in Figure 2) of the satellite.

the northern hemisphere on and around June solstice and then into the southern hemisphere during December solstice. This characteristic follows the fact that the Southern (Northern) hemisphere is in summer season during December (June) solstice, and the hemisphere experiencing summer receives the most solar radiation due to the longest period of daylight. A clear trend of increased WN structures of electron density in the northern summer hemisphere during solstices compared with that in winter hemisphere is evident throughout 2 year's WN1 profiles. Solar activity rises and falls with an 11-year cycle that affects ionospheric plasma density as well as the intensity of geomagnetic activity. The bottom panel of Figure 1 shows the 2-year patterns of solar radio flux F10.7, which is a common proxy for the level of photoionization in the earth's ionosphere, that is increasing from 2020 toward 2021. Also, strength of WN1 follows the trend of the amount of ionization caused by higher solar irradiance in the summer season, which occurs in June (December) in the northern (southern) hemisphere. These results strongly support the fact that the WN1 structure of the electron density has a significant seasonal dependence in the topside ionosphere.

The second panel of Figure 4 shows the latitudinal profile of WN2 structure of electron density for 2020 and 2021. WN2 seems to have equatorial symmetry with some sort of periodicity. Similarly, the third and bottom panels show the latitudinal profile of WN3 and WN4 of electron density for 2020 and 2021. In most of the cases, these profiles are equatorially symmetric, and maxima occur near southern hemispheric summer throughout the years. The sources and controlling factors behind the large-scale WN amplitudes structure of electron density will be discussed in detail in Section 4.

3.2. Swarm-C Neutral Density

Applying the method mentioned in Section 2.4, the absolute amplitudes of the WN1-WN4 are extracted using Equation 1 from Swam-C neutral density data for altitude range of 440 km. We evaluated all (WN1-WN4)

KHADKA ET AL. 10 of 23

21699402, 2024, 5, Downloaded from https://agupubs.onlinelibrary.wiley.com/doi/10.1029/2024JA032535 by Clemson University, Wiley Online Library on [28/04/2025]. See the Terms

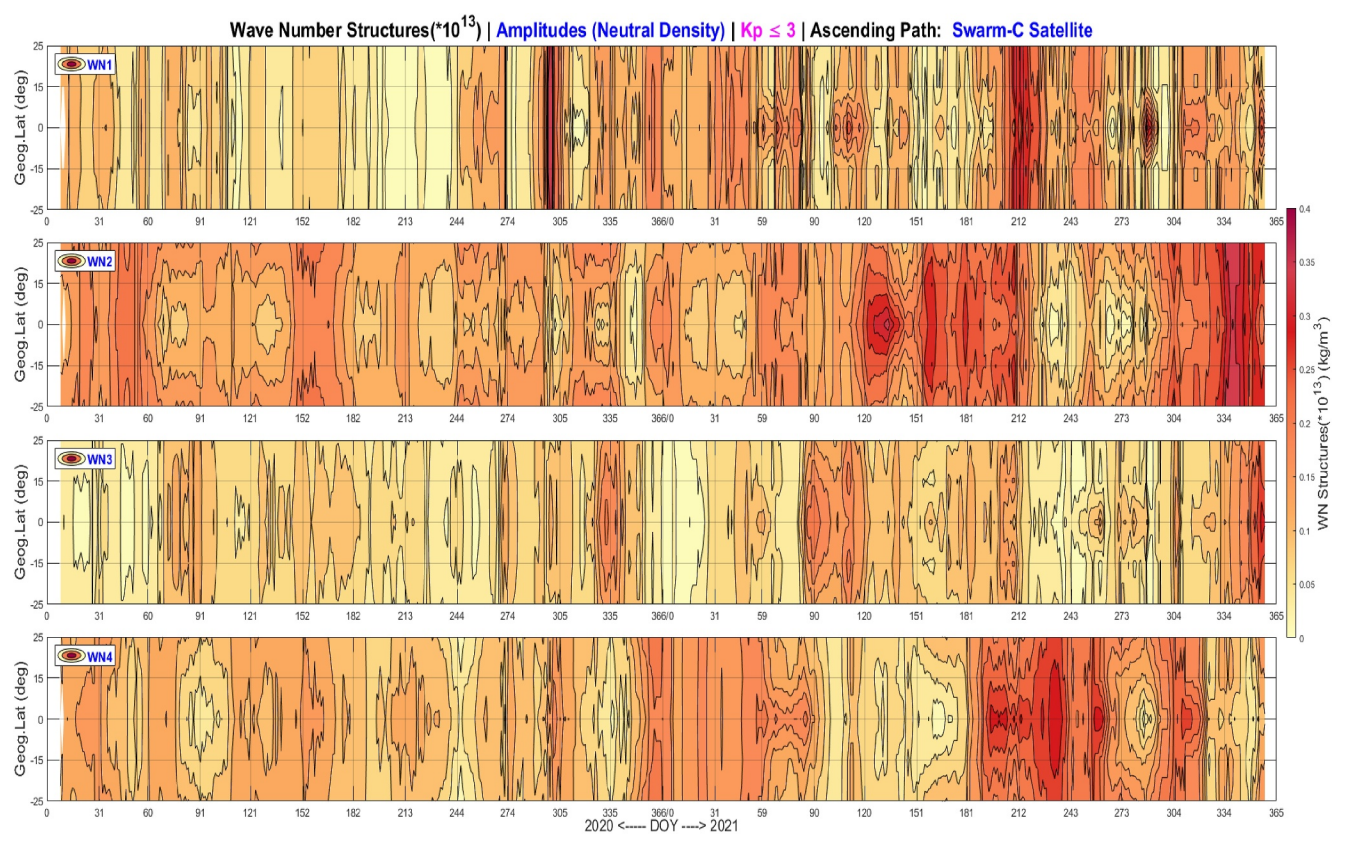


Figure 5. WNS from Swarm-C: Same contour (DOY vs. Geographic latitude) subplot of WN1-WN4 structures as Figure 4 but for neutral density data observed from Swarm-C satellite at 440 km altitude after highlighting symmetric structures.

amplitudes for the geographic latitudinal intervals, 20°N-30°N, 10°N-20°N, 10°N to 10°S, 10°S-20°S, and 20° S- 30° S that correspond to the amplitudes for $+25^{\circ}$, $+15^{\circ}$, 0° , -15° , and -25° , respectively. These neutraldensity WN amplitudes are represented as geographic latitude versus DOY contour subplots in Figure 5, which shows the distribution of the data at the low-latitudes. In order to highlight the equatorial latitudinal profiles of neutral density waves without any loss of information, we presented the amplitude variations in the symmetric parts of WN structures about the equator along the ascending path in Figure 5. We then evaluate the daily symmetric WN amplitudes of neutral density by summing the WN amplitudes in northern latitudes with those corresponding to southern latitudes, and then dividing the result by 2 to eliminate the antisymmetric components for ascending tracks of the satellite. Figure 5 characterizes the amplitude of WN structures obtained from neutral density observed in the middle thermosphere and the concurrent structure of electron density in the topside ionosphere is in Figure 4. Figure 5 shows the latitudinal profile of WN structures of neutral density for 2020 and 2021 and the profiles exhibit both symmetric as well as antisymmetric characteristics at different periods. The amplitudes of WN structures seem stronger in 2021 than during 2020. In May, June, July, and December of 2021, the amplitude of WN2 is equatorially symmetric and becomes stronger than that of other periods of the year. Also, right after June of 2021, WN4 increases abruptly for the 3 months of 2021. It can be inferred from Figure 5 that amplitude of WN2 neutral density dominates all other structures in 2020 and 2021.

3.3. Tidal Components From CTMT

We investigated diurnal and semidiurnal tidal variability in neutral density from the CTMT model to elucidate the relative contribution of the tidal components in the WN structures obtained from Swarm-C and DMSP-F18 data. We present the latitude-temporal structures of six diurnal and eight semidiurnal components of tidal density amplitude near 110 and 400 km altitudes because diurnal and semidiurnal tides are more predominant than other components. It is to be noted that CTMT only accounts for contributions from solar radiation absorption in the troposphere and stratosphere, tropospheric latent heat release, and non-linear wave-wave interactions occurring in

KHADKA ET AL. 11 of 23

the MLT or below. CTMT is unable to reproduce in situ-forced migrating tides resulting from solar EUV forcing (e.g., the middle thermospheric DW1), and in situ-forced nonmigrating tides in the middle thermosphere due to nonlinear interactions, most notably the diurnal nonmigrating tidal components DW2 and D0 that are likely forced by ion drag interactions at high latitudes (Jones et al., 2013). Figure 6 shows the contour plots of six diurnal and that of eight semidiurnal in Figure 7 tidal density amplitudes at (a) 110 km and (b) 400 km altitudes in the latitude versus month of the year (MOY) domains estimated from the Climatological Tidal Model of the Thermosphere (CTMT). The variability of six diurnal components (DW2, DW1, D0, DE1, DE2, and DE3) on latitude versus MOY is shown in Figure 6, and the variability of eight semidiurnal components (S0, SE1, SE2, SE3, SW1, SW2, SW3, and SW4) is shown in Figure 7. These components are evaluated from CTMT and quantitatively demonstrated for two altitudes, (a) 110 km and (b) 400 km.

From Figure 6, it is seen that the CTMT diurnal amplitude of relative density structures DE2, DE3, and DW2 reflect significant degree of symmetry about the equator at 110 km but DW2 is more symmetric at the lower heights (110 km) and more antisymmetric at the higher heights (400 km). The relative density is the ratio of the absolute density to the mean density, the annual and global mean densities are obtained from MSIS. The amplitude of equatorially symmetric DE3 is stronger than all of these. Further, the latitudinal distribution of DE3 centered near the equator is wider than other symmetric structures at 110 km as well as 400 km altitudes. Evidently, there is no significant change in the latitudinal structures of symmetric components of DE2 and DE3 tides at 110 km and at 400 km altitudes. It can be speculated that these tides propagate vertically into the thermosphere without suffering dissipation due to their longer vertical wavelengths. Primarily, D0 is antisymmetric about the equator and shows large maxima around $\pm 30^{\circ}$ latitude at 110 km which is further shifted toward the polar latitudes at 400 km altitude. The antisymmetric structure of DW1, the equatorial component at 110 km vanishes as one moves upward at 400 km.

An example of semidiurnal tidal signatures in the density is presented in Figure 7, which generally shows their peak amplitudes at higher latitudes/altitudes. The semidiurnal amplitude structures of density are nearly antisymmetric about the equator at both altitudes, 110, and 400 km, except SW4 which shows symmetric about equator at 400 km. SE1 has peak amplitudes at equator and at/around $\pm 60^{\circ}$ latitude during summer at both altitudes, 110, and 400 km. S0 amplitudes maximize at the poles whereas that of SW1 and SE2 maximize in the mid-latitude range. The maxima of SW3 occurs during equinox. Overall, the strength of SW2 dominates all other amplitudes at both altitudes of the analysis.

As listed in Table 1, the potential sources of WN1–WN4 are identified as tidal oscillations DW2, D0, SW1, SW3 and SPW1 for WN1; DW3, DE1, S0, SW4, and SPW2 for WN2; DE2, DW4, SE1, SW5, and SPW3 for WN3; and DE3, DW5, SE2, SW6 and SPW4 for WN4. We have reconstructed WN1–WN4 from corresponding potential sources available with CTMT. In the latitude versus MOY profile in Figure 8 shows the superposition of contributing CTMT component of tidal oscillations for WN1 to WN4 at 110 and 400 km altitudes. Only 11 tidal components obtained from CTMT are used for superposition plots in Figure 8. DW1, SE3, and SW2 are absent from depictions since CTMT provides 14 diurnal and semidiurnal components. Comparing 8(a) and 8(b), the WN4 is seen equatorially symmetric at 110 km but these patterns change to antisymmetric at 400 km altitude. But the nature of WN3 is exactly opposite that is, antisymmetric at 110 km but someway symmetric at 400 km. The reconstructed WN amplitudes in Figure 8 and their comparison with the observed amplitudes are discussed in the following sections.

Figure 8 suggests that the combined effect of migrating and nonmigrating tides are important for tidal modulation of the WN structures in the low latitude IT system. In terms of CTMT tidal components (shaded part in Table 1), WN1 is the aggregate effect of two diurnal (DW2, D0) and two semidiurnal (SW1 and SW3) components. These components are antisymmetric about the equator at 110 km and this anti-symmetry becomes clearer at 400 km. Similarly, WN2 and WN3, which have DE1, S0, and SW4 and DE2 and SE1 as potential sources respectively, are antisymmetric but the symmetric structure of WN3 is noticeable at 400 km. Interestingly, superposition of DE3 and SE2 generates equatorially symmetric WN4 structure at 110 km altitude that shifts toward the polar latitude at 400 km altitude, giving it an antisymmetric shape.

4. Interpretation and Discussion

Previous studies (e.g., Chang et al., 2011; Forbes & Roble, 1990; Forbes et al., 2021; Gasperini et al., 2015, 2021, 2023; Gu et al., 2014; He et al., 2011; Lieberman et al., 2022; Miyahara et al., 1993; Oberheide & Forbes, 2008;

KHADKA ET AL. 12 of 23

21699402, 2024, 5, Downloaded from https://agupubs.onlinelibrary.wiley.com/doi/10.1029/2024A032535 by Clemson University, Wiley Online Library on [28/04/2025]. See the Terms and Conditions (https://onlinelibrary.vibey.com/erms-and-conditions) on Wiley Online Library or rules of use; OA articles are governed by the applicable Creative Commons License

a)

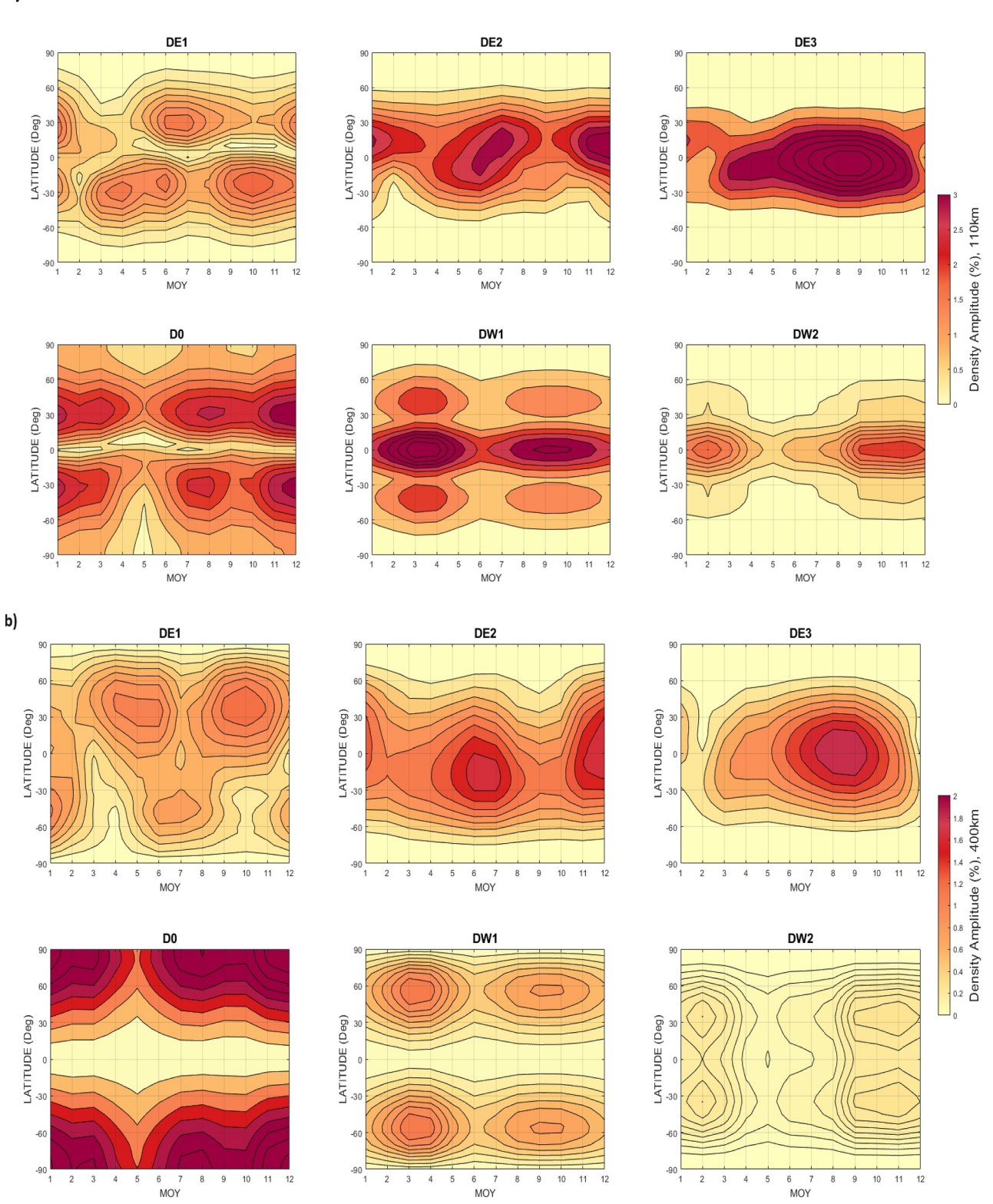


Figure 6. Diurnal Tidal Components from CTMT: Latitude versus month of the year (MOY) contours of diurnal amplitudes of density expressed in relative tides at (a) 110 km and (b) 400 km obtained from CTMT are shown. Diurnal tides, DE1, DE2, DE3, D0, DW1, and DW2 are depicted in those plots for both altitudes.

KHADKA ET AL. 13 of 23

2169902, 2024, 5, Downloaded from https://agupubs.onlinelibrary.wiley.com/doi/0.1029/2024/0.032535 by Clemson University, Wiley Online Library on [28/04/2025]. See the Terms and Conditions (https://onlinelibrary.wiley.com/terms-and-conditions) on Wiley Online Library for rules of use; OA articles are governed by the applicable Creating

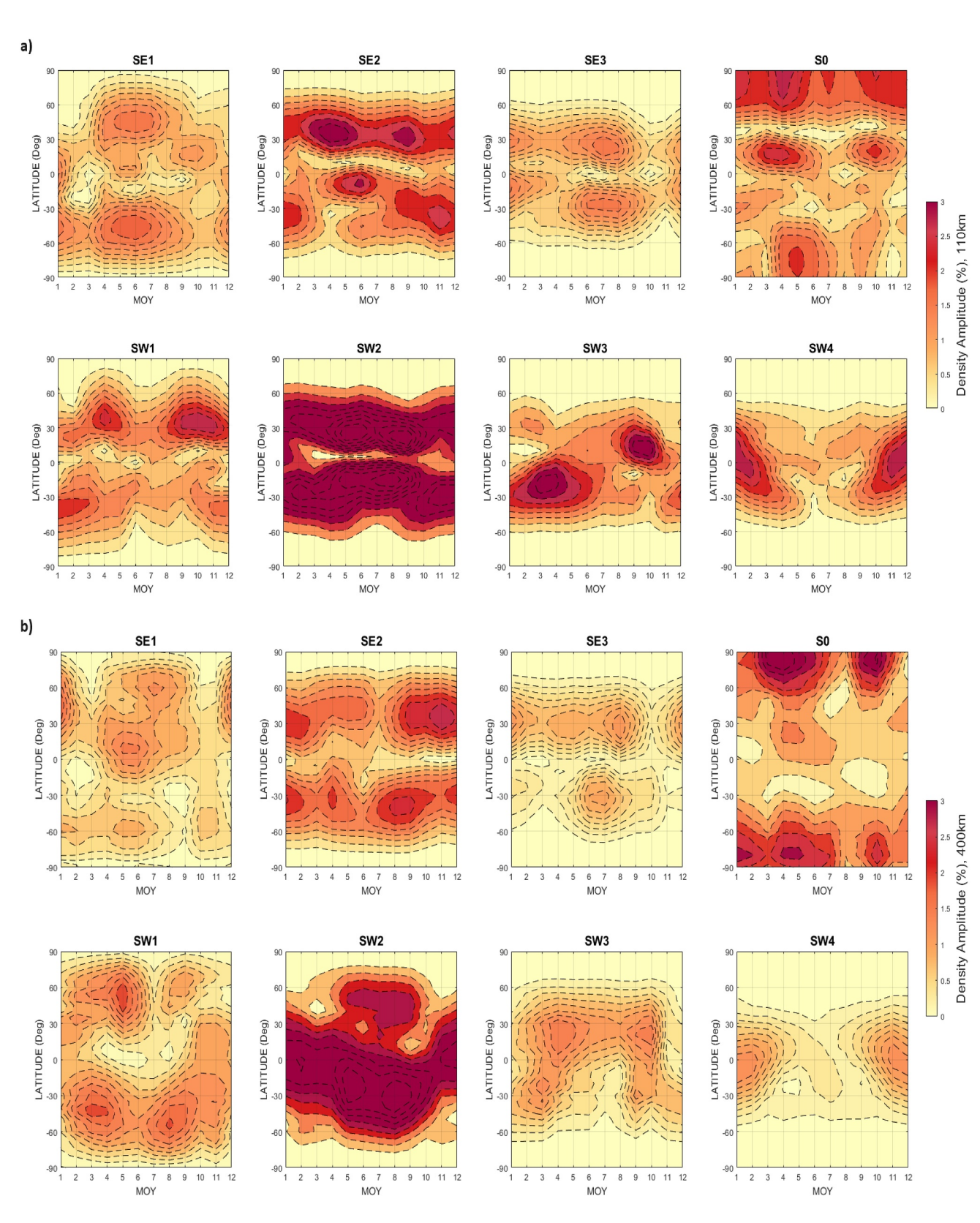


Figure 7. Semidiurnal Tidal Components from CTMT: Latitude-MOY contours of semidiurnal amplitudes of density expressed in relative tides at (a) 110 km and (b) 400 km altitudes obtained from the CTMT are shown. For semidiurnal tides, SE1, SE2, SE3, S0, SW1, SW2, SW3, and SW4 are depicted in those plots for both altitudes.

KHADKA ET AL. 14 of 23



2169902, 2024, 5, Downloaded from https://agupubs.onlinelibrary.wiley.com/doi/10.1029/2024/032535 by Clemson University, Wiley Online Library on [28/04/2025]. See the Terms and Conditions (https://onlinelibrary.wiley.com/ems-and-conditions) on Wiley Online Library for rules of use; OA articles are governed by the applicable Creative Creative Creative Conditions (https://onlinelibrary.wiley.com/ems-and-conditions) on Wiley Online Library for rules of use; OA articles are governed by the applicable Creative Creative Creative Creative Creative Conditions (https://onlinelibrary.wiley.com/ems-and-conditions) on Wiley Online Library for rules of use; OA articles are governed by the applicable Creative Creative

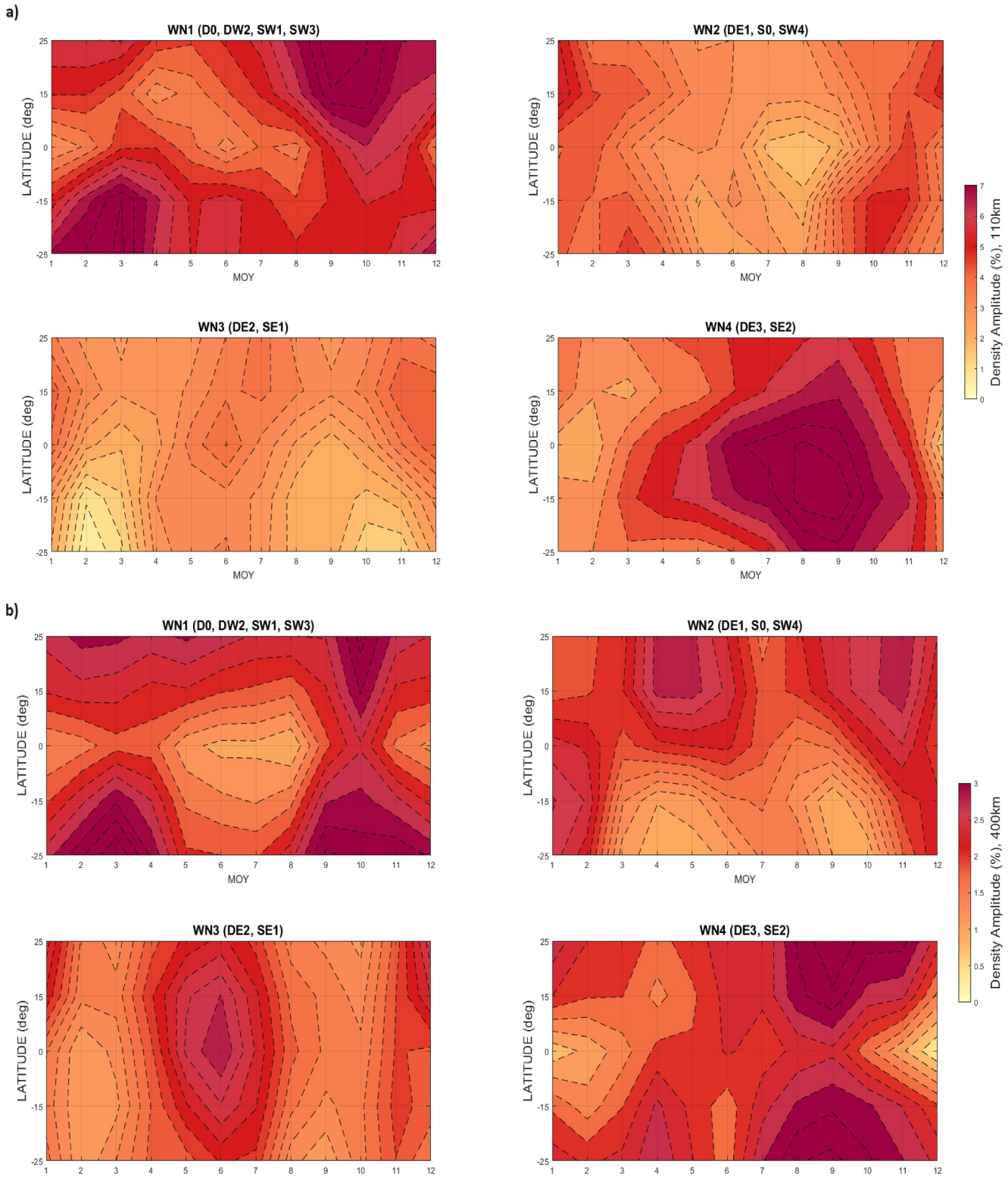


Figure 8. Superposition of CTMT Tidal Components as Sources of WN structures: A combined CTMT tidal components as potential sources of WN structures are depicted along latitude versus MOY contour plot, (a) for 110 km and (b) for 400 km altitudes. CTMT tidal oscillations D0, DW2, SW1, and SW3 are superposed for WN1. Similarly, DE1, S0, and SW4 are superposed for WN2; DE2 and SE1 for WN3; and DE3 and SE2 for WN4.

KHADKA ET AL. 15 of 23 Oberheide et al., 2015; Yiğit et al., 2016) demonstrated that upward propagating waves of tropospheric origin can have remarkable influences on interaction and coupling between large-scale wave structures in the low-latitude IT system. CTMT density (Oberheide et al., 2009) and temperature (Forbes et al., 2014) tides have already been extensively tested and validated with Challenging Minisatellite Payload (CHAMP) satellite data. Although our study is restricted to ±30° latitude, obvious evidence of modulation of the WN structures by the diurnal and semidiurnal migrating tides has been found in the lower thermosphere. It is useful to remember that this manuscript is about the WN structures evaluated from DMSP-F18 and Swarm-C observations with CTMT as a tool to identify the effect of upward propagating tides. We use CTMT output as latitude-temporal structures (14 diurnal and semidiurnal components) of tidal density amplitudes at 110 and 400 km altitudes. The principal influence of D0, DW2, SW1, and SW3 creates the WN1 structure. Referring to Figure 6, D0 is strongly antisymmetric about the equator at 110 km and such structure shifted toward polar latitude in CTMT and are not confined to low and middle latitudes. The aggregate effect of these tidal wave components likely forms the antisymmetric structure of WN1 (Figure 8) which can also be seen in the WN1 structures of electron density in DMSP-18 (Figure 4) and the neutral density in Swarm-C (Figure 5) data. DW2 and D0 have upper thermospheric sources and are generated in situ by a nonlinear interaction of DW1/SPW1 type (Oberheide et al., 2011a) whereas DW1 has a strong dependency on solar activity and season/latitude (Gasperini et al., 2023). SE2 can propagate from the troposphere. The middle/upper thermospheric DW2 is mostly due to magnetic/geographic pole displacements (from DW1, SPW1 interactions). A combined effect of DE1, S0, and SW4 contributes to WN2. Both CTMT and Swarm-C results show antisymmetric structure of WN2.

The contributors DE2 and SE1, account for the WN3 as the CTMT outputs in Figure 8. DE2 is a highly symmetric structure at both attitudes, 110, and 400 km. Whereas SE1 tidal structure is more antisymmetric with respect to the equator at 110 km as well as at 400 km. Overall, Swarm-C neutral density WN2 amplitude is also seen antisymmetric in structure. The DE2 tide is mainly generated by (a) latent heat release associated with deep tropical convection and (b) nonlinear interactions between migrating and non-migrating tides (England, 2012). From CTMT output perspective, the superposition of DE3 and SE2 is responsible for WN4. As seen in Figures 6 and 7, DE3 is symmetric and SE2 is antisymmetric at both altitudes, 110, and 400 km. In Figure 8, WN4 seems symmetric at 110 km even though it is antisymmetric at 400 km and gives an impression to depend on season/ MOY. It can be said that DE3 is a major contributor to the WN4 at 110 km altitude and can effectively propagate to the middle thermosphere, but SE2 takes the lead over DE3 at 400 km altitude. This is due to the higher frequency and the longer vertical wavelength of SE2 since this reduces the effects of dissipation compared to a diurnal tide (Oberheide et al., 2011a, 2011b). The strong symmetric WN4 structures of electron and neutral densities were also seen during similar period in Figures 4 and 5. Compared to all the individual tidal components, DE3 is the largest and is now known to produce significant ionospheric effects (Forbes et al., 2008). The antisymmetric structure of WN4 obtained from Swarm-C has been shifted toward higher latitudes in northern hemisphere which is clearly captured by the WN4 pattern of CTMT during August-September. In general, our CTMT results for the major potential sources of WN structures are qualitatively consistent with the satellite data.

Referring to Figure 2, in Figure 9, we choose the DOY 213-301 period in 2020 of mLT and LT ascending crossing node of the DMSP-F18 and Swarm-C satellites at low latitude ($\pm 10^{\circ}$) to observe the patterns of relative amplitude of electron and neutral density. Each row in Figure 9 shows the 7-day comparative plot of the relative WN1 to WN4 amplitudes of DMSP-F18 electron density (eD) and Swarm-C neutral density (nD) in LT 1 hr earlier, 1, 3, and 6 hr later than mLT, respectively. Excluding the 6 hr LT and mLT difference and those 3 hr difference for WN2, the patterns do not change much. Specifically, one can confirm from Figure 9 that if Swarm-C LT is 1 hr earlier than or 1 hr after the DMSP-F18 mLT along ascending path in the equatorial crossing of the satellites, the relative WN amplitude patterns look similar. The LT of the observed points on the ascending and descending orbit portions of a satellite is nearly independent of longitude (Lieberman et al., 2004; Oberheide et al., 2002). During the years 2020–2021, Swarm-C, with its slow precession orbit, covers approximately 24 hr of local time in a span of 133-135 days, considering both ascending and descending nodes. Consequently, these LT variation cycles are unlikely to significantly contribute to errors in the tidal extraction (Gasperini et al., 2015, 2017). When focusing solely on the ascending node of the satellite, it is reasonable to assume a fixed local time within moving windows for nonmigrating tidal extraction. Migrating tides, on the other hand, primarily arise from variations in the source and background atmosphere, as well as in situ forcing. The solar in situ forcing of migrating tides for dynamical changes in the upper thermosphere is not much more important than their upward propagating tidal components (Maute et al., 2023).

KHADKA ET AL. 16 of 23



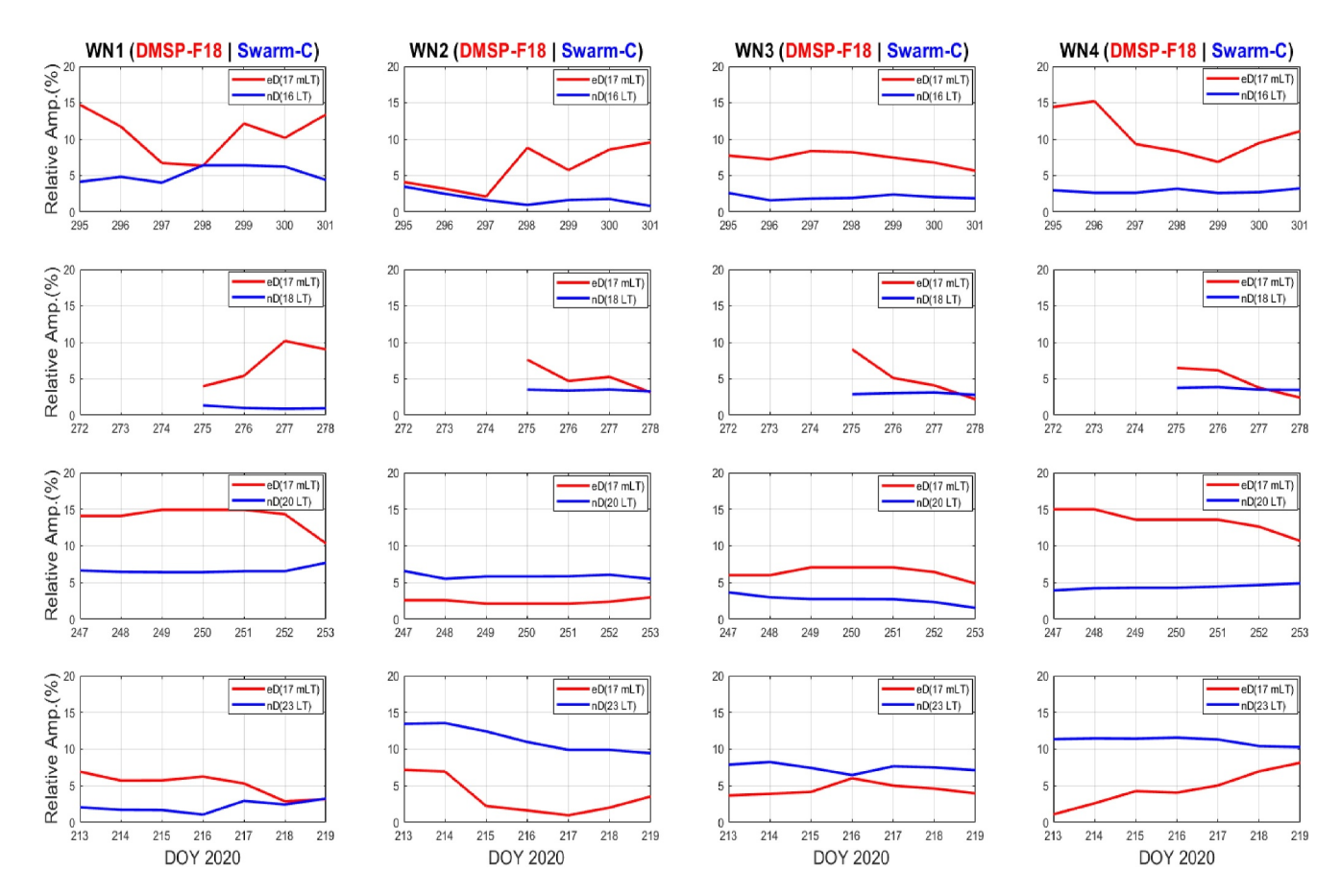


Figure 9. WN patterns in fixed mLT and different LT at Low Latitudes: Comparative patterns of relative WN amplitudes of DMSP-F18 electron density (eD) at 17 mLT and Swarm-C neutral density (nD) at different LT (16, 18, 20, 23) along ascending paths, that is, 1 hr earlier, 1, 3, and 6 hr later than mLT, respectively, within $\pm 10^{\circ}$ latitudes in 2020. The patterns exhibit similarity when there is a narrow difference between LT and mLT in most cases. Data gaps in the plot refer either unavailability of data or Kp > 3 days.

To investigate how the topside ionosphere responds to WN structures of neutral density and tidal components in the lower/middle thermosphere, we use two data sources, one providing topside ionospheric observations from DMSP-F18 and the other middle thermospheric observations from Swarm-C. We evaluate the Pearson's correlation coefficients between the WN structures in DMSP-F18 electron density and the Swarm-C neutral densities and then inspect the role of their potential tidal contributors of WN structures using CTMT results. The correlation coefficient is a statistical measure of linear dependence of two random variables, and the Pearson correlation coefficient is commonly used for the estimation of these parameters. It is difficult to accurately quantify correlation between parameters in the highly variable ionosphere that is involved in the complex process of interactions and IT coupling. Therefore, we have chosen 60-day moving windows for the analysis of correlation coefficients, that is, fourfold of moving windows (15-day) for WN structures analysis. The evaluated correlation coefficients between the WN structures of Swarm-C neutral density and the DMSP-F18 electron density are depicted in Figure 10 for 60-day moving windows in $\pm 10^{\circ}$ latitudes. We define a threshold value of ± 0.3 for correlation coefficients that are considered insignificant and not correlated well. Conversely, correlation coefficients greater than or equal to ± 0.6 are considered significant correlations.

There is strong evidence for the propagation of waves from 110 km to exosphere and can be measured tidal components, DE3, DE2, D0, SE2, SE3, and SE1. DW2, S0, SW4, and additional components are generated as in situ excitation components. (e.g., DW2, SW6) in the exosphere temperature (Forbes et al., 2014). Therefore, during the course of vertical propagation, these tidal components play a vital role in the interaction and coupling between WN structures in the middle thermosphere to topside ionosphere as their potential contributors. In terms of correlation coefficients, strong interactions can be defined as the coexistence of strong positive and negative

KHADKA ET AL. 17 of 23

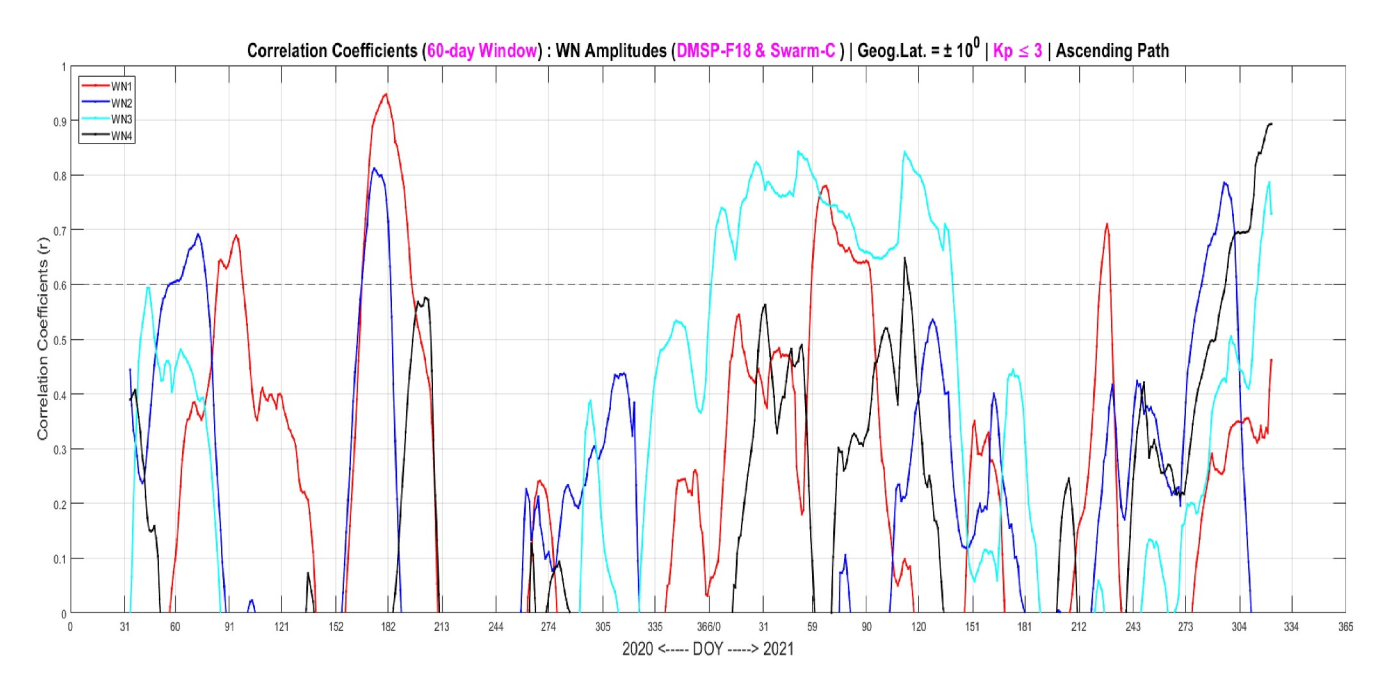


Figure 10. Correlation coefficients: Correlation coefficients between the electron and neutral density WN structures within $\pm 10^{\circ}$ geographic latitudes under sliding windows of 60-day sizes are shown. The red, blue, cyan, and black curves represent the correlation coefficients between the WN1, WN2, WN3, and WN4 of the DMSP-F18 electron and Swarm-C neutral density structures, respectively. We only consider positive correlation, which denotes the pattern of two variables moving in the same direction and is a suitable parameter to explain interactions and vertical coupling phenomena. Negative correlation coefficient values that refer to anti-correlation are set to null. The dotted horizontal lines represent correlation coefficient values equal to 0.6 and beyond that is considered as strong correlation between interacting wave WN structures.

correlation values among the interacting waves, such as tides, gravity waves, and planetary waves (Huang et al., 2012).

In Figure 10, the amplitudes of the WN1 structure of Swarm-C neutral density and DMSP-F18 electron density waves have very similar variations and intermittently highly correlated with more positive correlation events in 60-day windows. The significant positive correlation of WN1 is seen in March and April of both years, in June and July of 2020, and in August of 2021. Referring to Table 2 of Truskowski et al. (2014), spectra for the diurnal (D0 and DW2) and semidiurnal (SW1 and SW3) tides which are some of the contributors of WN1 are excited by both lower atmospheric heating as well as by non-linear wave-wave interactions. With this scenario, we may infer that the WN structures of electron density in topside ionosphere and those of neutral density in the middle thermosphere are highly correlated if their contributors as tidal components are excited by lower atmospheric heating, wave-wave interactions, and in situ excitation together.

From Figure 10, it can be perceived that for WN2, correlation is significant with positive values during March equinox and northern summer in 2020 but such patterns can be seen nearly end of 2021. Notably, the correlation between amplitude of the WN3 of Swarm-C neutral density and DMSP-F18 electron density is seen to possess almost equal, continuous, and significant positive correlation coefficient values during first 5 months of 2021.

The WN4 structures of electron density and that of neutral density show occasional positive correlation events with less than 0.6 value except during end of 2021. The longitudinal WN4 structure in the ionospheric F region originates from the symmetric modes of the DE3 tide in the ionospheric E region (Wan et al., 2010). Even though DE3 is symmetric at the equator (Figure 6), the combined effect of contributing tides for WN4 at higher altitude (Figure 8b) becomes antisymmetric. It can be suggested that if the vertical profile of contributing tidal components of WN structures is changing, weaker correlation is prevailed. For other intervals, correlation on WN structures occurs occasionally but not significantly.

KHADKA ET AL. 18 of 23

5. Summary and Conclusion

This study leads to a considerable advance in the study of the large-scale wave-driven interaction and plasmaneutral coupling in the low-latitude "IT gap" region. It also laid a few open and unresolved questions for future study. The outcomes presented here delineate how the wave number structures of thermospheric neutral density and topside ionospheric electron density interact with each other and respond to tidal components originating from the tropical troposphere. The tidal components obtained from an empirical climatological model display many characteristics related to interaction and coupling between the observed large-scale wave structures in this investigation. The major outcomes from our study are summarized as follows.

- Satellite observations of the WN structures of neutral and plasma density are the best way to examine largescale structures in the ionosphere-thermosphere (IT) system. The WN structures of Swarm-C neutral density in middle thermosphere and that of electron density measurement in the topside ionosphere from DMSP-F18 show the interaction and coupling processes between two altitudes.
- 2. The WN1 structure of the electron density has a significant seasonal dependence, like DW1, which is an interacting part of SPW1 that ultimately generates D0 and DW2 after interaction in the topside ionosphere. The antisymmetric patterns can clearly be seen in the magnitude of WN1 structure of electron density and seems to follow seasonal patterns in the low-latitude region. The stronger WN1 is seen extended into the northern hemisphere on and around June solstice and then into the southern hemisphere during December solstice. This characteristic follows the fact that the Southern (Northern) hemisphere is in summer season during December (June) solstice. The latitudinal profile of WN3 and WN4 of electron density for 2020 and 2021 look equatorially symmetric, and maxima occur near southern hemispheric summer throughout the years.
- 3. It also seems that WN2 neutral density amplitude dominates all other structures at around June solstice but WN1 and WN4 start to become prominent near the end of 2021. DE3 tides, which suffer less dissipation during vertical propagation, are the main contributor for WN4 structures at 110 km, but SE2 takes over its role at 400 km and can produce significant effects in the IT system.
- 4. The performance of the CTMT is an excellent model to explain vertical coupling phenomena caused by upward propagating tides from tropospheric sources with certain shortcomings. Even though all potential contributors of WN structures are not incorporated in CTMT, the available tidal components of CTMT can characterize the interaction and coupling process between WN structures. Notably, CTMT may overcome its limitations by assimilating Swarm-C data to better replicate the in situ forced tides.
- 5. This study confirms that tides act as key agents of interaction and coupling between the large-scale wave-number structure of neutral density in the lower thermosphere and the electron density in the topside ionosphere. If Swarm-C LT is 1 hr earlier than or 1 hr after the DMSP-F18 mLT along ascending path in the equatorial crossing of satellites, the relative WN amplitude patterns look similar. WN structures of electron density in topside ionosphere and those of neutral density in the middle thermosphere are highly correlated if their contributors as tidal components are excited by lower atmospheric heating, wave-wave interactions, and in situ excitation together in the low-latitude region.
- 6. Comparison of observation and model reveal that the diurnal and semidiurnal nonmigrating tides propagate directly upward from their terrestrial source regions, which can modulate the WN structures in the low-latitude IT region creating the constructive and destructive interference effects among potential sources of the WN structures along their vertical propagation.
- 7. There is a remarkable (>0.6) but intermittent correlation between WN structures of Swarm-C neutral density and DMSP-F18 electron density. Amplitudes of the WN1 and WN3 structures have significant correlation events than that of the WN2 and WN4 throughout 2020 and 2021 in 60-day sliding windows analysis.

To sum up, this study highlights the importance of the "IT gap" region and attempts to examine the topside ionospheric response to wave driving in the lower atmosphere from tidal perspectives. Simultaneous and multisatellites observations improve the capability to resolve large-scale features and understanding interaction and vertical coupling in the "IT gap" from tropospheric sources to advance our abilities on satellite operations and space weather. More research efforts of IT phenomena are necessary to improve space situational awareness (SSA) to secure and advance technology-based modern society. Meanwhile, NASA's upcoming missions, the Geospace Dynamics Constellation (GDC), consisting of six satellite constellations is scheduled to be co-launched with the Dynamical Neutral Atmosphere-Ionosphere Coupling (DYNAMIC) mission around 2030 which are aimed to investigate basically how and why tidal weather vary, respectively (Oberheide et al., 2023). These missions will undoubtedly make significant progress in addressing not only how terrestrial weather processes

KHADKA ET AL. 19 of 23



Journal of Geophysical Research: Space Physics

10.1029/2024JA032535

produce space weather effects but also in providing insights to update and improve current modeling approaches in the IT system for the heliophysics community.

Data Availability Statement

Data sets and climatological model used in this study are publicly available. The geomagnetic Kp index, Ap index, and F10.7 Solar Radio Flux data are available at https://kp.gfz-potsdam.de/en/data. The DMSP ion density data are available via the CEDAR Madrigal Database at http://cedar.openmadrigal.org/. The Swarm-C Precise Orbit Determination (POD)-derived neutral density product are available at http://thermosphere.tudelft.nl/. The neutral density data from the Swarm-C satellite pertinent to this paper can be found at https://doi.org/10.5281/zenodo.11107142 (Khadka, 2024). CTMT is available from http://dx.doi.org/10.5281/zenodo.5541913 (Oberheide, 2011).

Acknowledgments

FG and SK acknowledge support from the AFOSR award number FA9550-22-1-0328 and NASA Grants 80NSSC22K0019 and 80NSSC22K1010. JO acknowledges support by NASA Grants 80NSSC20K1353, 80NSSC22K0018, 80NSSC22K1010, and through the NSF ANSWERS program, award 2149695.

References

- Cahoy, K. L., Hinson, D. P., & Tyler, G. L. (2006). Radio science measurements of atmospheric refractivity with Mars Global Surveyor. *Journal of Geophysical Research*, 111(E5), E05003. https://doi.org/10.1029/2005JE002634
- Cai, Y., Yue, X., Wang, W., Zhang, S., Liu, L., Liu, H., & Wan, W. (2019). Long-term trend of topside ionospheric electron density derived from DMSP data during 1995–2017. *Journal of Geophysical Research: Space Physics*, 124(12), 10708–10727. https://doi.org/10.1029/ 2019JA027522
- Chang, L., Palo, S., Hagan, M., Richter, J., Garcia, R., Riggin, D., & Fritts, D. (2008). Structure of the migrating diurnal tide in the whole atmosphere community climate model (WACCM). Advances in Space Research, 41(9), 1398–1407. https://doi.org/10.1016/j.asr.2007.03.035
- Chang, L. C., Lin, C.-H., Yue, J., Liu, J.-Y., & Lin, J.-T. (2013). Stationary planetary wave and nonmigrating tidal signatures in ionospheric wave 3 and wave 4 variations in 2007–2011 FORMOSAT-3/COSMIC observations. *Journal of Geophysical Research: Space Physics*, 118(10), 6651–6665. https://doi.org/10.1002/jgra.50583
- Chang, L. C., Liu, J.-Y., & Palo, S. E. (2011). Propagating planetary wave coupling in SABER MLT temperatures and GPS TEC during the 2005/2006 austral summer. *Journal of Geophysical Research*, 116(A10), A10324. https://doi.org/10.1029/2011JA016687
- England, S. L. (2012). A review of the effects of non-migrating atmospheric tides on the Earth's low-latitude ionosphere. *Space Science Reviews*, 168(1–4), 211–236. https://doi.org/10.1007/s11214-011-9842-4
- England, S. L., Immel, T. J., & Huba, J. D. (2008). Modeling the longitudinal variation in the post-sunset far-ultraviolet OI airglow using the SAMI2 model. *Journal of Geophysical Research*, 113(A1), A01309. https://doi.org/10.1029/2007JA012536
- Fang, T.-W., Akmaev, R., Fuller-Rowell, T., Wu, F., Maruyama, N., & Millward, G. (2013). Longitudinal and day-to-day variability in the ionosphere from lower atmosphere tidal forcing. Geophysical Research Letters, 40(11), 2523–2528. https://doi.org/10.1002/grl.50550
- Forbes, J. M. (2000). Wave coupling between the lower and upper atmosphere: Case study of an ultra-fast Kelvin wave. *Journal of Atmospheric and Terrestrial Physics*, 62(17–18), 1603–1621. https://doi.org/10.1016/s1364-6826(00)00115-2
- Forbes, J. M., & Garrett, H. B. (1979). Theoretical studies of atmospheric tides. Reviews of Geophysics, 17(8), 1951–1981. https://doi.org/10.1029/RG017i008p01951
- Forbes, J. M., & Hagan, M. E. (1982). Thermospheric extensions of the classical expansion functions for semidiurnal tides. *Journal of Geophysical Research*, 87(A7), 5253–5259. https://doi.org/10.1029/JA087iA07p05253
- Forbes, J. M., Maute, A., Zhang, X., & Hagan, M. E. (2018). Oscillation of the ionosphere at planetary-wave periods. *Journal of Geophysical Research: Space Physics*, 123(9), 7634–7649. https://doi.org/10.1029/2018JA025720
- Forbes, J. M., Oberheide, J., Zhang, X., Cullens, C., Englert, C. R., Harding, B. J., et al. (2022). Vertical coupling by solar semidiumnal tides in the thermosphere from ICON/MIGHTI measurements. *Journal of Geophysical Research: Space Physics*, 127(5), e2022JA030288. https://doi.org/ 10.1029/2022JA030288
- Forbes, J. M., & Roble, R. G. (1990). Thermosphere-ionosphere coupling: An experiment in interactive modeling. *Journal of Geophysical Research*, 95(A1), 201–208. https://doi.org/10.1029/ja095ia01p00201
- Forbes, J. M., & Wu, D. (2006). Solar tides as revealed by measurements of mesosphere temperature by the MLS experiment on UARS. *Journal of the Atmospheric Sciences*, 63(7), 1776–1797. https://doi.org/10.1175/jas3724.1
- Forbes, J. M., Zhang, X., & Bruinsma, S. (2012). Middle and upper thermosphere density structures due to nonmigrating tides. *Journal of Geophysical Research*, 117(A11), A11306. https://doi.org/10.1029/2012JA018087
- Forbes, J. M., Zhang, X., & Bruinsma, S. L. (2014). New perspectives on thermosphere tides: 2. Penetration to the upper thermosphere. *Earth Planets and Space*, 66(1), 122. https://doi.org/10.1186/1880-5981-66-122
- Forbes, J. M., Zhang, X., Hagan, M. E., England, S. L., Liu, G., & Gasperini, F. (2017). On the specification of upward-propagating tides for ICON science investigations. Space Science Reviews, 212(1–2), 697–713. https://doi.org/10.1007/s11214-017-0401-5
- Forbes, J. M., Zhang, X., Heelis, R., Stoneback, R., Englert, C. R., Harlander, J. M., et al. (2021). Atmosphere-ionosphere (A-I) coupling as viewed by ICON: Day-to-day variability due to planetary wave (PW)-tide interactions. *Journal of Geophysical Research: Space Physics*, 126(6), e2020JA028927. https://doi.org/10.1029/2020JA028927
- Forbes, J. M., Zhang, X., Palo, S., Russell, J., Mertens, C. J., & Mlynczak, M. (2008). Tidal variability in the ionospheric dynamo region. *Journal of Geophysical Research*, 113(A2), A02310. https://doi.org/10.1029/2007JA012737
- Forbes, J. M., Zhang, X. L., Palo, S. E., Russell, J., Mertens, C. J., & Mlynczak, M. (2009). Kelvin waves in stratosphere, mesosphere and lower thermosphere temperatures as observed by TIMED/SABER during 2002–2006. Earth Planets and Space, 61(4), 447–453. https://doi.org/10. 1186/bf03353161
- Friis-Christensen, E., Lühr, H., Knudsen, D., & Haagmans, R. (2008). Swarm—An Earth observation mission investigating geospace. Advances in Space Research, 41(1), 210–216. https://doi.org/10.1016/j.asr.2006.10.008
- Fritts, D. C., & Alexander, M. J. (2003). Gravity wave dynamics and effects in the middle atmosphere. Reviews of Geophysics, 41, 1003. https://doi.org/10.1029/2001RG000106

KHADKA ET AL. 20 of 23

- Garner, T. W., Taylor, B. T., Gaussiran, T. L., Coley, W. R., Hairston, M. R., & Rich, F. J. (2010). Statistical behavior of the topside electron density as determined from DMSP observations: A probabilistic climatology. *Journal of Geophysical Research*, 115(A7), A07306. https://doi. org/10.1029/2009JA014695
- Gasperini, F., Azeem, I., Crowley, G., Perdue, M., Depew, M., Immel, T., et al. (2021). Dynamical coupling between the low-latitude lower thermosphere and ionosphere via the non-migrating diurnal tide as revealed by concurrent satellite observations and numerical modeling. *Geophysical Research Letters*, 48(14), e2021GL093277. https://doi.org/10.1029/2021GL093277
- Gasperini, F., Crowley, G., Immel, T. J., & Harding, B. J. (2022). Vertical wave coupling in the low-latitude ionosphere-thermosphere as revealed by concurrent ICON and COSMIC-2 observations. *Space Science Reviews*, 218(7), 55. https://doi.org/10.1007/s11214-022-00923-1
- Gasperini, F., Forbes, J. M., Doornbos, E. N., & Bruinsma, S. L. (2015). Wave coupling between the lower and middle thermosphere as viewed from TIMED and GOCE. *Journal of Geophysical Research: Space Physics*, 120(7), 5788–5804. https://doi.org/10.1002/2015JA021300
- Gasperini, F., Forbes, J. M., Doornbos, E. N., & Bruinsma, S. L. (2018). Kelvin wave coupling from TIMED and GOCE: Inter/intra-annual variability and solar activity effects. *Journal of Atmospheric and Solar-Terrestrial Physics*, 171, 176–187. https://doi.org/10.1016/j.jastp.2017.08.034
- Gasperini, F., Hagan, M. E., & Zhao, Y. (2017). Evidence of tropospheric 90 day oscillations in the thermosphere. Geophysical Research Letters, 44(20), 10125–10133. https://doi.org/10.1002/2017gl075445
- Gasperini, F., Harding, B. J., Crowley, G., & Immel, T. J. (2023). Ionosphere-thermosphere coupling via global-scale waves: New insights from two-years of concurrent in situ and remotely-sensed satellite observations. Frontiers in Astronomy and Space Sciences, 10. https://doi.org/10. 3389/fspas.2023.1217737
- Gong, Y., & Zhou, Q. (2011). Incoherent scatter radar study of the terdiurnal tide in the E- and F-region heights at Arecibo. *Geophysical Research Letters*, 38(15), L15101. https://doi.org/10.1029/2011GL048318
- Gu, S.-Y., Liu, H.-L., Li, T., Dou, X., Wu, Q., & Russell, J. M., III. (2014). Observation of the neutral-ion coupling through 6 day planetary wave. Journal of Geophysical Research: Space Physics, 119(12), 10376–10383. https://doi.org/10.1002/2014JA020530
- Hagan, M. E., & Forbes, J. M. (2002). Migrating and nonmigrating diurnal tides in the middle and upper atmosphere excited by tropospheric latent heat release. *Journal of Geophysical Research*, 107(D24), 4754. https://doi.org/10.1029/2001JD001236
- Hagan, M. E., Maute, A., Roble, R. G., Richmond, A. D., Immel, T. J., & England, S. L. (2007). Connections between deep tropical clouds and the Earth's ionosphere. *Geophysical Research Letters*, 34(20), L20109. https://doi.org/10.1029/2007GL030142
- Hagan, M. E., & Roble, R. G. (2001). Modeling diurnal tidal variability with the national center for atmospheric research thermosphere–ionosphere–mesosphere–electrodynamics general circulation model. *Journal of Geophysical Research*, 106(A11), 24869–24882. https://doi.org/10.1029/2001ja000057
- Hairston, M. R., & Heelis, R. A. (1996). *Analysis of ionospheric parameters based on DMSP SSIES data using the DBASE4 and NADIA programs*Tech. Rep. Phillips Laboratory, Directorate of Geophysics, Hanscom Air Force Base, Massachusetts.
- Hairston, M. R., Heelis, R. A., & Rich, F. J. (1998). Analysis of the ionospheric cross polar cap potential drop using DMSP data during the National Space Weather Program study period. *Journal of Geophysical Research*, 103(A11), 26337–26347. https://doi.org/10.1029/071A03241
- Häusler, K., & Lühr, H. (2009). Nonmigrating tidal signals in the upper thermospheric zonal wind at equatorial latitudes as observed by CHAMP. Annales Geophysicae, 27(7), 2643–2652. https://doi.org/10.5194/angeo-27-2643-2009
- He, M., Liu, L., Wan, W., & Wei, Y. (2011). Strong evidence for couplings between the ionospheric wave-4 structure and atmospheric tides. Geophysical Research Letters, 38(14), L14101. https://doi.org/10.1029/2011GL047855
- Huang, C., Zhang, S., Zhou, Q., Yi, F., & Huang, K. (2012). Atmospheric waves and their interactions in the thermospheric neutral wind as observed by the Arecibo incoherent scatter radar. *Journal of Geophysical Research*, 117(D19), D19105. https://doi.org/10.1029/ 2012JD018241
- Immel, T. J., England, S. L., Mende, S. B., Heelis, R. A., Englert, C. R., Edelstein, J., et al. (2018). The ionospheric connection explorer mission: Mission goals and design. Space Science Reviews. 214(1), 13. https://doi.org/10.1007/s11214-017-0449-2
- Jaén-Vargas, M., Reyes Leiva, K. M., Fernandes, F., Barroso Gonçalves, S., Tavares Silva, M., Lopes, D. S., & Serrano Olmedo, J. J. (2022).
 Effects of sliding window variation in the performance of acceleration-based human activity recognition using deep learning models. *PeerJ Computer Science*, 8, e1052. PMID: 36091986; PMCID: PMC9455026. https://doi.org/10.7717/peerj-cs.1052
- Jarvis, M. (2006). Planetary wave trends in the lower thermosphere Evidence for 22-year solar modulation of the quasi-5-day wave. *Journal of Atmospheric and Solar-Terrestrial Physics*, 68(17), 1902–1912. https://doi.org/10.1016/j.jastp.2006.02.014
- Jones, M., Forbes, J. M., Hagan, M. E., & Maute, A. (2014). Impacts of vertically propagating tides on the mean state of the ionosphere-thermosphere system. *Journal of Geophysical Research: Space Physics*, 119(3), 2197–2213. https://doi.org/10.1002/2013JA019744
- Jones, M., Jr., Forbes, J. M., Hagan, M. E., & Maute, A. (2013). Non-migrating tides in the ionosphere-thermosphere: In situ versus tropospheric sources. *Journal of Geophysical Research: Space Physics*, 118(5), 2438–2451. https://doi.org/10.1002/jgra.50257
- Jones, M., Jr., Forbes, J. M., & Sassi, F. (2019). The effects of vertically propagating tides on the mean dynamical structure of the lower thermosphere. *Journal of Geophysical Research: Space Physics*, 124(8), 7202–7219. https://doi.org/10.1029/2019JA026934
- Khadka, S. M. (2024). Swarm-C neutral density data for large-scale wave (LSW) structures [Dataset]. Zenodo. https://doi.org/10.5281/zenodo. 11107142
- Khadka, S. M. (2018). Multi-diagnostic investigations of the equatorial and low-latitude ionospheric electrodynamics and their impacts on space-based technologies Ph.D. Dissertation. Retrieved from http://hdl.handle.net/2345/bc-ir:108001
- Khadka, S. M., Valladares, C., Pradipta, R., Pacheco, E., & Condor, P. (2016). On the mutual relationship of the equatorial electrojet, TEC and scintillation in the Peruvian sector. Radio Science, 51(6), 742–751. https://doi.org/10.1002/2016RS005966
- Kil, H., Lee, W. K., Shim, J., Paxton, L. J., & Zhang, Y. (2013). The effect of the 135.6 nm emission originated from the ionosphere on the TIMED/GUVI O/N2 ratio. *Journal of Geophysical Research: Space Physics*, 118(2), 859–865. https://doi.org/10.1029/2012JA018112
- Kramer, H. J. (2002). Observation of the Earth and its environment: Survey of missions and sensors (4th ed. 2002, p. 1514). Springer Verlag. Krier, C. S., England, S. L., Greer, K. R., Evans, J. S., Burns, A. G., & Eastes, R. W. (2021). Deducing non-migrating diurnal tides in the middle thermosphere with GOLD observations of the Earth's far ultraviolet dayglow from geostationary orbit. Journal of Geophysical Research: Space Physics, 126(10), e2021JA029563. https://doi.org/10.1029/2021JA029563
- Lawrence, A. R., & Jarvis, M. J. (2001). Initial comparisons of planetary waves in the stratosphere, mesosphere and ionosphere over Antarctica. Geophysical Research Letters, 28(2), 203–206. https://doi.org/10.1029/2000g1000116
- Lawrence, A. R., & Jarvis, M. J. (2003). Simultaneous observations of planetary waves from 30 to 220 km. Journal of Atmospheric and Solar-Terrestrial Physics, 65(6), 765–777. https://doi.org/10.1016/s1364-6826(03)00081-6
- Lieberman, R. S., Harding, B. J., Heelis, R. A., Pedatella, N. M., Forbes, J. M., & Oberheide, J. (2022). Atmospheric lunar tide in the low latitude thermosphere-ionosphere. *Geophysical Research Letters*, 49(11), e2022GL098078. https://doi.org/10.1029/2022GL098078

KHADKA ET AL. 21 of 23



Journal of Geophysical Research: Space Physics

- 10.1029/2024JA032535
- Lieberman, R. S., Oberheide, J., Hagan, M. E., Remsberg, E. E., & Gordley, L. L. (2004). Variability of diurnal tides and planetary waves during November 1978–May 1979, 2004. *Journal of Atmospheric and Solar-Terrestrial Physics*, 66(6–9), 517–528. https://doi.org/10.1016/j.jastp. 2004.01.006
- Lieberman, R. S., Oberheide, J., & Talaat, E. R. (2013). Nonmigrating diurnal tides observed in global thermospheric winds. *Journal of Geophysical Research: Space Physics*, 118(11), 7384–7397. https://doi.org/10.1002/2013JA018975
- Lin, C. H., Wang, W., Hagan, M. E., Hsiao, C. C., Immel, T. J., Hsu, M. L., et al. (2007). Plausible effect of atmospheric tides on the equatorial ionosphere observed by the FORMOSAT-3/COSMIC: Three-dimensional electron density structures. *Geophysical Research Letters*, 34(11), L11112. https://doi.org/10.1029/2007GL029265
- Liu, G., Immel, T. J., England, S. L., Frey, H. U., Mende, S. B., Kumar, K. K., & Ramkumar, G. (2013). Impacts of atmospheric ultrafast Kelvin waves on radio scintillations in the equatorial ionosphere. *Journal of Geophysical Research: Space Physics*, 118(2), 885–891. https://doi.org/10.1002/jgra.50139
- Liu, G., Lieberman, R. S., Harvey, V. L., Pedatella, N. M., Oberheide, J., Hibbins, R. E., et al. (2021). Tidal variations in the mesosphere and lower thermosphere before, during, and after the 2009 sudden stratospheric warming. *Journal of Geophysical Research: Space Physics*, 126(3), e2020JA028827. https://doi.org/10.1029/2020JA028827
- Matzka, J., Stolle, C., Yamazaki, Y., Bronkalla, O., & Morschhauser, A. (2021). The geomagnetic Kp index and derived indices of geomagnetic activity. Space Weather, 19(5), e2020SW002641. https://doi.org/10.1029/2020SW002641
- Maute, A., Forbes, J. M., Cullens, C. Y., & Immel, T. J. (2023). Delineating the effect of upward propagating migrating solar tides with the TIEGCM-ICON. Frontiers in Astronomy and Space Sciences, 10, 1147571. https://doi.org/10.3389/fspas.2023.1147571
- McLandress, C. (2002). The seasonal variation of the propagating diurnal tide in the mesosphere and lower thermosphere: Part II. The role of tidal heating and zonal mean winds. *Journal of the Atmospheric Sciences*, 59(5), 907–922. https://doi.org/10.1175/1520-0469(2002)059<0907: tsvotp>2.0.co;2
- McLandress, C., Shepherd, G. G., & Solheim, B. H. (1996). Satellite observations of thermospheric tides: Results from the wind imaging interferometer on UARS. *Journal of Geophysical Research*, 101(D2), 4093–4114. https://doi.org/10.1029/95JD03359
- Miyahara, S., Yoshida, Y., & Miyoshi, Y. (1993). Dynamic coupling between the lower and upper atmosphere by tides and gravity waves. *Journal of Atmospheric and Terrestrial Physics*, 55(7), 1039–1053. https://doi.org/10.1016/0021-9169(93)90096-H
- Molina, I., & Scherliess, L. (2023). Longitudinal variability of thermospheric zonal winds near dawn and dusk. Frontiers in Astronomy and Space Sciences, 10, 1214612. https://doi.org/10.3389/fspas.2023.1214612
- Mukhtarov, P., & Pancheva, D. (2011). Global ionospheric response to nonmigrating DE3 and DE2 tides forced from below. *Journal of Geophysical Research*, 116(A5), A05323. https://doi.org/10.1029/2010JA016099
- Negrea, C., Zabotin, N., Bullett, T., Codrescu, M., & Fuller-Rowell, T. (2016). Ionospheric response to tidal waves measured by dynasonde
- techniques. *Journal of Geophysical Research: Space Physics*, 121(1), 602–611. https://doi.org/10.1002/2015JA021574 Oberheide, J. (2011). Climatological tidal model of the thermosphere—CTMT (Version 1) [Dataset]. *Zenodo*. https://doi.org/10.5281/zenodo.
- Oberheide, J., & Forbes, J. M. (2008). Tidal propagation of deep tropical cloud signatures into the thermosphere from TIMED observations.
- Geophysical Research Letters, 35(4), L04816. https://doi.org/10.1029/2007GL032397

 Oberheide, J., Forbes, J. M., Hausler, K., Wu, Q., & Bruinsma, S. L. (2009). Tropospheric tides from 80 to 400 km: Propagation, interannual
- variability, and solar cycle effects. *Journal of Geophysical Research*, 114(D1), D00I05. https://doi.org/10.1029/2009JD012388

 Oberheide, J., Forbes, J. M., Zhang, X., & Bruinsma, S. L. (2011a). Climatology of upward propagating diurnal and semidiurnal tides in the
- thermosphere. *Journal of Geophysical Research*, 116(A11), A11306. https://doi.org/10.1029/2011JA016784

 Oberheide, J., Forbes, J. M., Zhang, X., & Bruinsma, S. L. (2011b). Wave-driven variability in the ionosphere-thermosphere-mesosphere system
- from TIMED observations: What contributes to the "wave 4". *Journal of Geophysical Research*, 116(A1), A01306. https://doi.org/10.1029/2010JA015911
- Oberheide, J., Gardner, S. M., & Neogi, M. (2023). Resolving the tidal weather of the thermosphere using GDC. Frontiers in Astronomy and Space Sciences, 10, 1282261. https://doi.org/10.3389/fspas.2023.1282261
- Oberheide, J., Hagan, M. E., Roble, R. G., & Offermann, D. (2002). Sources of nonmigrating tides in the tropical middle atmosphere. *Journal of Geophysical Research*, 107(D21), 4567. https://doi.org/10.1029/2002JD002220
- Oberheide, J., Shiokawa, K., Gurubaran, S., Ward, W. E., Fujiwara, H., Kosch, M. J., et al. (2015). The geospace response to variable inputs from the lower atmosphere: A review of the progress made by Task Group 4 of CAWSES-II. *Progress in Earth and Planetary Science*, 2(1), 2. https://doi.org/10.1186/s40645-014-0031-4
- Pedatella, N. M., & Forbes, J. M. (2009). Interannual variability in the longitudinal structure of the low-latitude ionosphere due to the El Niño–Southern Oscillation. *Journal of Geophysical Research*, 114(A12), A12316. https://doi.org/10.1029/2009JA014494
- Pedatella, N. M., Forbes, J. M., Lei, J., Thayer, J. P., & Larson, K. M. (2008). Changes in the longitudinal structure of the low-latitude ionosphere during the July 2004 sequence of geomagnetic storms. *Journal of Geophysical Research*, 113(A11), A11315. https://doi.org/10.1029/ 2008JA013539
- Pirscher, B., Foelsche, U., Borsche, M., Kirchengast, G., & Kuo, Y.-H. (2010). Analysis of migrating diurnal tides detected in FORMOSAT-3/COSMIC temperature data. *Journal of Geophysical Research*, 115(D14), D14108. https://doi.org/10.1029/2009JD013008
- Qian, L., Gan, Q., Wang, W., Cai, X., Eastes, R., & Yue, J. (2022). Seasonal variation of thermospheric composition observed by NASA GOLD. Journal of Geophysical Research: Space Physics, 127(6), e2022JA030496. https://doi.org/10.1029/2022JA030496
- Sato, K., Watanabe, S., Kawatani, Y., Tomikawa, Y., Miyazaki, K., & Takahashi, M. (2009). On the origins of mesospheric gravity waves. Geophysical Research Letters, 36(19), L19801. https://doi.org/10.1029/2009GL039908
- Schrijver, C. J., Kauristie, K., Aylward, A. D., Denardini, C. M., Gibson, S. E., Glover, A., et al. (2015). Understanding space weather to shield society: A global road map for 2015–2025 commissioned by COSPAR and ILWS. Advances in Space Research, 55(12), 2745–2807. https://doi.org/10.1016/j.asr.2015.03.023
- Siemes, C., de Teixeira da Encarnação, J., Doornbos, E., van den IJssel, J., Kraus, J., Pereštý, R., et al. (2016). Swarm accelerometer data processing from raw accelerations to thermospheric neutral densities. *Earth Planets and Space*, 68(1), 92. https://doi.org/10.1186/s40623-016-0474-5
- Smith, A. K. (2003). The origin of stationary planetary waves in the upper mesosphere. *Journal of the Atmospheric Sciences*, 60(24), 3033–3041. https://doi.org/10.1175/1520-0469(2003)060<3033:toospw>2.0.co;2
- Smith, A. K. (2012). Global dynamics of the MLT. Surveys in Geophysics, 33(6), 1177-1230. https://doi.org/10.1007/s10712-012-9196-9
- Svoboda, A. A., Forbes, J. M., & Miyahara, S. (2005). A space-based climatology of diurnal MLT tidal winds, temperatures and densities from UARS wind measurements. *Journal of Atmospheric and Solar-Terrestrial Physics*, 67(16), 1533–1543. https://doi.org/10.1016/j.jastp.2005.08.01

KHADKA ET AL. 22 of 23



Journal of Geophysical Research: Space Physics

- 10.1029/2024JA032535
- Triplett, C. C., Immel, T. J., Wu, Y. J., & Cullens, C. (2019). Variations in the ionosphere-thermosphere system from tides, ultra-fast Kelvin waves, and their interactions. *Advances in Space Research*, 64(10), 1841–1853. Epub 2019 Aug 23. PMID: 33867620; PMCID: PMC8050945. https://doi.org/10.1016/j.asr.2019.08.015
- Truskowski, A. O., Forbes, J. M., Zhang, X., & Palo, S. E. (2014). New perspectives on thermosphere tides: 1. Lower thermosphere spectra and seasonal-latitudinal structures. *Earth Planets and Space*, 66, 136. https://doi.org/10.1186/s40623-014-0136-4
- van den IJssel, J., Doornbos, E., Iorfida, E., March, G., Siemes, C., & Montenbruck, O. (2020). Thermosphere densities derived from Swarm GPS observations. Advances in Space Research, 65(7), 1758–1771. https://doi.org/10.1016/j.asr.2020.01.004
- Vincent, R. A. (2015). The dynamics of the mesosphere and lower thermosphere: A brief review. *Progress in Earth and Planetary Science*, 2(1), 4. https://doi.org/10.1186/s40645-015-0035-8
- Visser, P., Doornbos, E., van den IJssel, J., & Teixeira da Encarnação, J. (2013). Thermospheric density and wind retrieval from Swarm observations. Earth Planets and Space, 65(11), 12–1331. https://doi.org/10.5047/eps.2013.08.003
- Wan, W., Xiong, J., Ren, Z., Liu, L., Zhang, M.-L., Ding, F., et al. (2010). Correlation between the ionospheric WN4 signature and the upper atmospheric DE3 tide. *Journal of Geophysical Research*, 115(A11), A11303. https://doi.org/10.1029/2010JA015527
- Wang, J. C., Palo, S. E., Liu, H.-L., & Siskind, D. E. (2021). Day-to-day variability of diurnal tide in the mesosphere and lower thermosphere driven from below. *Journal of Geophysical Research: Space Physics*, 126(2), e2019JA027759. https://doi.org/10.1029/2019JA027759
- Williams, C. R., & Avery, S. K. (1996). Diurnal nonmigrating tidal oscillations forced by deep convective clouds. *Journal of Geophysical Research*, 101(D2), 4079–4091. https://doi.org/10.1029/95JD03007
- Wood, A. G., Alfonsi, L., Clausen, L. B. N., Jin, Y., Spogli, L., Urbář, J., et al. (2022). Variability of ionospheric plasma: Results from the ESA Swarm mission. Space Science Reviews, 218(6), 52. https://doi.org/10.1007/s11214-022-00916-0
- Wu, Q., Ortland, D. A., Killeen, T. L., Roble, R. G., Hagan, M. E., Liu, H.-L., et al. (2008). Global distribution and interannual variations of mesospheric and lower thermospheric neutral wind diurnal tide: 2. Nonmigrating tide. *Journal of Geophysical Research*, 113(A5), A05309. https://doi.org/10.1029/2007JA012543
- Yamazaki, Y., Harding, B. J., Qiu, L., Stolle, C., Siddiqui, T. A., Miyoshi, Y., et al. (2023). Monthly climatologies of zonal-mean and tidal winds in the thermosphere as observed by ICON/MIGHTI during April 2020–March 2022. Earth and Space Science, 10(6), e2023EA002962. https://doi.org/10.1029/2023EA002962
- Yamazaki, Y., & Richmond, A. D. (2013). A theory of ionospheric response to upward-propagating tides: Electrodynamic effects and tidal mixing effects. *Journal of Geophysical Research: Space Physics*, 118(9), 5891–5905. https://doi.org/10.1002/jgra.50487
- Yiğit, E., Knížová, P. K., Georgieva, K., & Ward, W. (2016). A review of vertical coupling in the atmosphere-ionosphere system: Effects of waves, sudden stratospheric warmings, space weather, and of solar activity. *Journal of Atmospheric and Solar-Terrestrial Physics*, 141, 1–12. https://doi.org/10.1016/j.jastp.2016.02.011
- Yuan, T., Stevens, M. H., Englert, C. R., & Immel, T. J. (2021). Temperature tides across the mid-latitude summer turbopause measured by a sodium lidar and MIGHTI/ICON. *Journal of Geophysical Research: Atmospheres*, 126(16), e2021JD035321. Epub 2021 Aug 11. PMID: 34777927; PMCID: PMC8587882. https://doi.org/10.1029/2021jd035321
- Yue, J., Wang, W., Richmond, A. D., Liu, H.-L., & Chang, L. C. (2013). Wavenumber broadening of the quasi 2 day planetary wave in the ionosphere. *Journal of Geophysical Research: Space Physics*, 118(6), 3515–3526. https://doi.org/10.1002/jgra.50307
- Yue, J., Wang, W., Ruan, H., Chang, L. C., & Lei, J. (2016). Impact of the interaction between the quasi-2 day wave and tides on the ionosphere and thermosphere. *Journal of Geophysical Research: Space Physics*, 121(4), 3555–3563. https://doi.org/10.1002/2016JA022444
- Zeng, Z., Randel, W., Sokolovskiy, S., Deser, C., Kuo, Y.-H., Hagan, M., et al. (2008). Detection of migrating diurnal tide in the tropical upper troposphere and lower stratosphere using the Challenging Minisatellite Payload radio occultation data. *Journal of Geophysical Research*, 113(D3), D03102. https://doi.org/10.1029/2007JD008725
- Zhang, X., Forbes, J. M., & Hagan, M. E. (2012). Seasonal-latitudinal variation of the eastward-propagating diurnal tide with zonal wavenumber 3 in the MLT: Influences of heating and background wind distribution. *Journal of Atmospheric and Solar-Terrestrial Physics*, 78–79, 37–43. https://doi.org/10.1016/j.jastp.2011.03.005
- Zhang, X., Forbes, J. M., Hagan, M. E., Russell, J. M., III., Palo, S. E., Mertens, C. J., & Mlynczak, M. G. (2006). Monthly tidal temperatures 20–120 km from TIMED/SABER. *Journal of Geophysical Research*, 111(A10), A10S08. https://doi.org/10.1029/2005JA011504

KHADKA ET AL. 23 of 23